Submitted to AmMin in 2022, **ms8596, Revision 2**

Twinning in hydrous wadsleyite: symmetry relations, origin, and consequences

Nobuyoshi Miyajima[1], Johannes Buchen[1,2] and Takaaki Kawazoe[1,3]

[1] Bayerisches Geoinstitut, Universität Bayreuth, 95440 Germany

[2] Department of Earth Sciences, University of Oxford, Oxford OX1 3AN, United Kingdom

[3] Earth and Planetary Systems Science Program, Graduate School of Advanced Science and Engineering, Hiroshima University, Higashi-Hiroshima, 739-8526, Japan

Miyajima, Nobuyoshi Nobuyoshi.Miyajima@uni-bayreuth.de

Johannes Buchen johannes.buchen@earth.ox.ac.uk

Takaaki KAWAZOE kawazoe@hiroshima-u.ac.jp

Abstract:

Twins in hydrous wadsleyite were detected by polarized-light microscopy and characterized with transmission electron microscopy techniques including precession selected area electron diffraction and large-angle convergent beam diffraction. By inspecting diffracted intensities for high-order Laue zones, we found the symmetry of our hydrous wadsleyite samples to be reduced to monoclinic with respect to the orthorhombic symmetry of most anhydrous wadsleyite samples.

Twinned domains in hydrous wadsleyite share the (122) plane as composition plane and are related to each other by a two-fold rotation around a twin axis parallel to [212] or by reflection on (122). The twin axis and twin plane in wadsleyite correspond to the <101> directions and the {101} planes of ringwoodite, respectively. The twin operations exchange the c^* and the [120]* directions of wadsleyite, both of which correspond to the directions of the cubic a axes in ringwoodite. Based on our analysis of symmetry relations and pseudo-symmetry in wadsleyite, we conclude that the twins formed during crystal growth under quasi-hydrostatic conditions in the presence of a hydrous fluid. Twinning in wadsleyite may affect the physical properties and deformation behavior of wadsleyite as well as the phase transition to ringwoodite in the Earth's mantle transition zone.

Keywords

Twinning, hydrous wadsleyite, transmission electron microscopy, Earth's mantle transition zone

Introduction

As a high-pressure polymorph of the mineral olivine, wadsleyite (β-$(Mg,Fe)_2SiO_4$) is expected to be a major mineral in peridotitic lithologies in the upper part of the transition zone of Earth's mantle at depths between 410 and 520 km (e.g., Frost, 2008). Despite numerous studies on the physical properties (e.g., Buchen et al., 2017; Zhou et al., 2021) and crystal-chemical characteristics (e.g., Smyth et al., 2014; Kawazoe et al., 2016) of wadsleyite, little is known about the morphology of wadsleyite. Morphological properties, such as crystal shape, cleavage, and twinning, however, can impact the physical response of polycrystalline aggregates, in particular when interacting with the anisotropic properties of individual grains or domains. Here we report on the discovery of twinning in hydrous wadsleyite and determine the twin law by combining transmission electron microscopy with a theoretical analysis of symmetry relations.

Anhydrous wadsleyite most frequently crystallizes with orthorhombic symmetry (space-group type *Imma*, Moore and Smith, 1970; Horiuchi and Sawamoto, 1981). The crystal structure of wadsleyite (wds) is closely related to the cubic spinel structure of ringwoodite (rwd), another high-pressure polymorph of olivine. Both structures can be described by different stacking sequences of structural modules along the $[010]_{wds}$ or $[110]_{rwd}$ directions (Price, 1983; Price et al., 1983; Putnis, 1992). In the presence of H_2O, wadsleyite incorporates hydrogen in the form of hydroxyl groups (Inoue et al., 1995; Kohlstedt et al., 1996; McKay et al., 2019). The incorporation of hydroxyl groups into wadsleyite and the related formation of cation vacancies may reduce the crystal symmetry of wadsleyite to monoclinic (space-group type $I2/m$) with $\beta \neq 90°$ (Smyth et al., 1997). This change in symmetry can be described by the loss of the mirror plane perpendicular to the *a* axis due to partial ordering of vacancies on octahedral sites (Smyth et al., 1997; Kudoh and Inoue, 1999). Holl et al. (2008) reported broadening and possible peak

splitting of the 244 diffraction peak of a hydrous wadsleyite crystal by performing omega scans along the *a*, b**, and *c** directions on a four-circle diffractometer (Figure 7 in Holl et al., 2008). They attributed the observed peak splitting to polysynthetic twinning, but did not specify any twin relations. The existence of twins in wadsleyite, however, has not yet been demonstrated by using electron microscopy techniques. Here we report, for the first time, twinning in synthetic hydrous Fe-bearing wadsleyite. We first detected the twins in thin sections of wadsleyite samples by the change in color across twin boundaries, which is enhanced by the strong pleochroism of Fe-bearing wadsleyite when viewed under a polarized-light microscope (**Fig. 1**). To further characterize the twinning, we used transmission electron microscopy (TEM) assisted with electron diffraction and scanning transmission electron beam techniques. Based on our observations, we derive the twin law and discuss the origin of the twins in hydrous wadsleyite.

Experimental procedures

Sample synthesis at high pressure and temperature

Polycrystalline wadsleyite samples were synthesized from a powder made from San Carlos olivine and saturated with distilled water. The wet powder was filled into a platinum capsule, compressed to a pressure of 15 GPa, and held at a temperature of 1670 K for 3 h using a Kawai-type multi-anvil apparatus at the Bayerisches Geoinstitut, Universität Bayreuth. Further details about the synthesis procedure have been described in Kawazoe et al. (2015). The obtained crystals were several hundred micrometers in length, but less than 1 mm. The ratio Fe/(Mg+Fe) was determined by electron microprobe analysis to be 0.097(1). The water content was determined by infrared spectroscopy (sample H4183 in Buchen, 2018) and corresponds to about

This is the peer-reviewed, final accepted version for American Mineralogist, published by the Mineralogical Society of America.
The published version is subject to change. Cite as Authors (Year) Title. American Mineralogist, in press.
DOI: https://doi.org/10.2138/am-2022-8596. http://www.minsocam.org/

79 0.72 wt% H_2O (equivalent to 0.058 H_2O molecules per formula unit). The unit cell parameters of
80 a twinned wadsleyite crystal (Fig. 1b) were determined from 33 X-ray reflections, which were
81 centered on a four-circle diffractometer with a point detector and a Mo *K*α X-ray source operated
82 at 40 kV and 30 mA. We refined the unit cell parameters assuming first orthorhombic and then
83 monoclinic symmetry (**Table 1**).

84 ***Transmission electron microscopy***

85 Two thin foils, one of which perpendicular to the twin boundary, were cut from a twinned
86 wadsleyite crystal with a dual-beam focused ion beam (FIB) milling machine (FEI Scios) (**Fig.**
87 **2**). The two extracted TEM thin foils were oriented normal to the $[2\bar{1}0]_{wds}$ ($<100>_{rwd}$) and
88 $[001]_{wds}$ ($<001>_{rwd}$) zone axes, respectively, and were inspected with scanning transmission
89 electron microscopes (FEI Titan G2 80-200 S/TEM and Philips CM20FEG) operating at 200 kV.
90 The foil perpendicular to the $[2\bar{1}0]_{wds}$ zone axis was prepared with the intention of identifying
91 the twin relation by using precession selected area electron diffraction (PsSAED) and large-angle
92 convergent beam diffraction (LACBED) techniques. The foil perpendicular to the $[001]_{wds}$ zone
93 axis was intended to investigate a potential symmetry reduction from the orthorhombic (point
94 group *mmm*) to the monoclinic structure (2/*m*) (Smyth et al., 1997; Holl et al., 2008) by using
95 high-order Laue zones (HOLZ) in the selected area electron diffraction (SAED) pattern. For
96 comparison, a HOLZ pattern of the $[\bar{1}10]$ zone axis of olivine was recorded with the same
97 microscope. Scanning moiré fringe (SMF) imaging by scanning transmission electron
98 microscopy (STEM) (Su and Zhu, 2010) has, for the first time, been applied to a high-pressure
99 mineral to visualize a change of moiré fringe pattern across the composition plane at a relatively
100 low electron dose due to lower magnification (a 160 k times magnification), about 70 times
101 lower than that of a conventional magnification (at 1300 k times) under high resolution STEM

conditions (usually at 1000-5000 k times). The chemical homogeneity at the composition plane was investigated in high-resolution TEM (HRTEM) and analytical STEM combined with a high-angle annular dark field (HAADF) detector. The HRTEM image presented was processed using a Wiener filter which was implemented in a Gatan DigitalMicrograph (Mitchell and Schaffer, 2005) to remove noise contrast (Kilaas, 1998).

Results

Investigation of the twin relation by transmission electron microscopy

The TEM observations assisted with SAED revealed that the orientations of twin domains can be brought into coincidence by a 180° rotation about an axis nearly perpendicular to the $(122)_{wds}$ plane in wadsleyite or by reflection on the $(122)_{wds}$ plane, which corresponds to one of the $\{101\}_{rwd}$ planes in the cubic system, i.e., a cubic axis system attached to structural units in common with the cubic structure of ringwoodite (**Figs. 3 and 8 and Supplemental Information Figs. S1 and S2**). Therefore, potential twin elements include a two-fold twin axis nearly perpendicular to the $(122)_{wds}$ plane and a mirror plane parallel to $(122)_{wds}$, or to one of the $\{122\}_{wds}$ planes in orthorhombic symmetry and hereafter denoted as $(122)_{wds}$ for simplicity. The SAED patterns from twin-related domains display these symmetry relations (**Supplemental Figs. S1 and S2**). SAED patterns of the twin boundary recorded along the $[2\bar{1}0]_{wds}$ zone axis show that 244 reflections (and higher orders) are split along the direction perpendicular to the twin boundary (**Fig. 3**). For non-zero obliquity, reflections are typically split along a direction normal to the composition plane, i.e., the plane shared by two adjacent domains. The splitting of reflections therefore indicates that the composition plane is parallel to one of the $\{244\}_{wds}$ planes

This is the peer-reviewed, final accepted version for American Mineralogist, published by the Mineralogical Society of America.
The published version is subject to change. Cite as Authors (Year) Title. American Mineralogist, in press.
DOI: https://doi.org/10.2138/am-2022-8596. http://www.minsocam.org/

and hence parallel to $(122)_{wds}$. This observation is consistent with the splitting and broadening of 244 reflections reported by Holl et al. (2008). During our single-crystal X-ray diffraction experiments, we observed a similar splitting of 244 reflections in omega scans of a twinned wadsleyite crystal (**Supplemental Fig. S3**).

Apart from the splitting of 244 diffraction spots in SAED patterns, we did not observe significant orientational misfits or remarkable discontinuities of the Bragg lines in the LACBED pattern recorded in the vicinity of the composition plane (**Fig. 4**). With the exception of a visible discontinuity along the composition plane, we did not detect visible structural defects such as dislocation arrays or chemical differences in the vicinity of or across the twin boundary in the conventional high-resolution lattice TEM image (**Fig. 5a),** by SMF-STEM (**Figs. 5b and 5c**), or by HAADF-STEM imaging (**Supplemental Fig. S4**).

Space-group identification and symmetry reduction

The electron diffraction pattern along the $[001]_{wds}$ zone axis is crucial for identifying a potential reduction from orthorhombic to monoclinic symmetry (space-group type $I2/m$, b as unique axis). In the diffraction pattern, the reflection conditions for $hk0$ reflections and the existence of a mirror plane perpendicular to the a axis should be verified to distinguish between monoclinic and orthorhombic symmetries. Reflections for $\mathbf{g} = hk0$: $h, k = 2n + 1$ are forbidden by the orthorhombic space group *Imma* but not by the monoclinic space group $I2/m$ reported for hydrous wadsleyite by Smyth et al. (1997). **Figure 6a** displays SAED patterns of the $[001]_{wds}$ zone axis without any detectable intensities of $hk0$ reflections with $h, k = 2n + 1$, while the intensity of the 110 reflection was detected in a systematic diffraction condition along the [110]* direction (**Fig. 6b**). In **Fig. 6b**, however, some dynamical diffraction effects, e.g., double

This is the peer-reviewed, final accepted version for American Mineralogist, published by the Mineralogical Society of America.
The published version is subject to change. Cite as Authors (Year) Title. American Mineralogist, in press.
DOI: https://doi.org/10.2138/am-2022-8596. http://www.minsocam.org/

diffraction, might be visible. To test for mirror symmetries along the *a* and *b* axes, the intensity distributions of high-order Laue zones for the $[001]_{wds}$ zone axis were also examined to confirm the absence of a mirror plane perpendicular to the *a* axis by using SAED patterns with smaller camera lengths (**Fig. 7 and Supplemental Fig. S5**). In the HOLZ pattern of the $[001]_{wds}$ zone axis using a reduced camera length of 340 mm, the intensity distributions along the a^* axis are asymmetric, while those along the *b* axis are symmetric, which points to the absence of a mirror plane perpendicular to the *a* axis, consistent with the monoclinic space group $I2/m$ (unique axis *b*) but not with the orthorhombic space group *Imma*, i.e., $I\,2/m\,2/m\,2/a$. In addition, the intensity distributions of the Bragg lines in a LACBED pattern of the $[001]_{wds}$ zone axis were also examined to test for the existence of a mirror plane perpendicular to the *a* axis (**Supplemental Fig. S6**). In conclusion, our detailed analysis of diffracted intensities with TEM suggests our wadsleyite samples to be monoclinic, consistent with the significant deviation of the angle β from 90° as detected by single-crystal X-ray diffraction (**Table 1**).

Discussion

Symmetry analysis of twins in hydrous wadsleyite and derivation of the twin law

Our TEM observations suggest that individual twin domains in hydrous wadsleyite are related to each other by reflection on $(122)_{wds}$ or by a two-fold rotation about a twin axis nearly perpendicular to one of the $(122)_{wds}$ planes. Mallard's law requires the twin axis to be a lattice element in direct space. Since the direction $[212]_{wds}$, or an equivalent thereof, is the lattice row closest to be perpendicular to a $(122)_{wds}$ plane, this direction is a good candidate for the orientation of the twin axis. Indeed, exploring potential twin operations in the realm of the

This is the peer-reviewed, final accepted version for American Mineralogist, published by the Mineralogical Society of America.
The published version is subject to change. Cite as Authors (Year) Title. American Mineralogist, in press.
DOI: https://doi.org/10.2138/am-2022-8596. http://www.minsocam.org/

reticular theory of twinning (Grimmer & Nespolo, 2006) by running the program *GEMINOGRAPHY* (Nespolo & Ferraris, 2006) on the monoclinic unit cell given in **Table 1** proposes the pair of twin elements $(122)_{wds}$ and $[212]_{wds}$. According to this theory, twinning in hydrous wadsleyite is by reticular pseudo-merohedry or, more specifically, by reticular pseudo-polyholohedry with the unique axis of the *I*-centered pseudo-monoclinic twin lattice (TL) oriented along the $[212]_{wds}$ direction of wadsleyite. The twin lattice can be described by the parameters a_{TL} = 14.076 Å, b_{TL} = 23.137 Å, c_{TL} = 14.169 Å, α_{TL} = 89.26°, β_{TL} = 110.06°, γ_{TL} = 91.25°. The orientation of the axes spanning the twin lattice expressed relative to the crystal axes of wadsleyite is given by the matrix:

$$\mathbf{T} = \begin{bmatrix} 2 & 2 & 0 \\ 0 & 1 & -1 \\ -1 & 2 & 1 \end{bmatrix}$$

The second column of the matrix **T** is the direction of the twin axis in direct space expressed in coordinates of the crystal axis system of wadsleyite, the first and third columns are the shortest independent vectors parallel to the $(122)_{wds}$ twin plane, respectively. The associated obliquity, i.e., the orientational mismatch between twin domains, is 1.29°, and the twin index is 8. The theoretical analysis of twin operations is therefore fully consistent with our TEM observations, including the minor orientational mismatch as reflected in the splitting of 244 diffraction spots in SAED patterns.

To derive the twin law, we need to find the cosets of the point group of the twin lattice by decomposition with respect to the intersection group of the point groups of the individual domains in their relative orientations. As the twin operations do not map any of the mirror planes or twofold axes of the orthorhombic point group *mmm* of one twin domain onto their counterparts in another domain, the intersection group *H* of the individuals only contains the

This is the peer-reviewed, final accepted version for American Mineralogist, published by the Mineralogical Society of America.
The published version is subject to change. Cite as Authors (Year) Title. American Mineralogist, in press.
DOI: https://doi.org/10.2138/am-2022-8596. http://www.minsocam.org/

identity operation and inversion, $H = \{1, \bar{1}\} = \bar{1}$. The point group of the twin lattice is a supergroup of the intersection group and needs to contain the twin operations and reflect the symmetry of the twin lattice. When we neglect the small obliquity and assume the twin lattice to be monoclinic, these conditions are met by the point group G of the twin lattice with $G = \{1, \bar{1}, 2, m\}$, i.e., $G = 2/m$. The coset decomposition of G with respect to H then yields the cosets $\{1, \bar{1}\}$ and $\{2, m\}$, the first of which is the intersection group H. The symmetry operations of reflection on $(122)_{wds}$ and two-fold rotation around $[212]_{wds}$ as detected by our TEM work and confirmed by symmetry analysis therefore constitute the twin law.

Relation to ringwoodite

Both a two-fold rotation around $[212]_{wds}$ and reflection on $(122)_{wds}$ map the c^* axis of one twin domain onto the [120]* direction of another twin domain. Each of these directions corresponds to one of the cubic a axes (a_1, a_2, or a_3) of ringwoodite. Similarly, both twin operations map the $\{101\}_{wds}$ set of planes onto the $\{021\}_{wds}$ set of planes, both of which correspond to the $\{111\}_{rwd}$ planes in ringwoodite. In both minerals, close-packed layers of oxygen anions are oriented parallel to the respective families of planes. The twin operations therefore map the oxygen substructure onto itself. The relation between the crystal structures of wadsleyite and ringwoodite is illustrated in **Figure 8**. A vector **w** with coordinates w_1, w_2, w_3 defined with respect to the crystal axes of wadsleyite is transformed to a vector **r** in the cubic axis system of ringwoodite by the matrix (see **Supplemental Information**)

$$\mathbf{Mw} = \frac{1}{2}\begin{bmatrix} 1 & 2 & 0 \\ -1 & 2 & 0 \\ 0 & 0 & 2 \end{bmatrix}\begin{pmatrix} w_1 \\ w_2 \\ w_3 \end{pmatrix} = \begin{pmatrix} r_1 \\ r_2 \\ r_3 \end{pmatrix} = \mathbf{r}$$

This is the peer-reviewed, final accepted version for American Mineralogist, published by the Mineralogical Society of America.
The published version is subject to change. Cite as Authors (Year) Title. American Mineralogist, in press.
DOI: https://doi.org/10.2138/am-2022-8596. http://www.minsocam.org/

209 The twin lattice is then related to the crystal axes of ringwoodite by the matrix

$$\mathbf{MT} = \begin{bmatrix} 1 & 2 & -1 \\ -1 & 0 & -1 \\ -1 & 2 & 1 \end{bmatrix}$$

210 In terms of the axis system of ringwoodite, the twin lattice is spanned by two space diagonals
211 through the unit cell and the face diagonal that is perpendicular to both of them. The two-fold
212 twin axis is oriented along this face diagonal, i.e., along $[101]_{rwd}$. Note that while a two-fold
213 rotation around $[101]_{rwd}$ is not a symmetry operation of the spinel structure of ringwoodite
214 (space-group type $F\bar{4}3m$), reflection on the plane perpendicular to $[101]_{rwd}$, i.e., on $(101)_{rwd}$, is
215 indeed a symmetry operation of ringwoodite. The symmetry characteristics of twins in hydrous
216 wadsleyite might therefore indicate a structural relation to ringwoodite.

217

218 ***Origin of twins in wadsleyite***

219 The twins we detected in wadsleyite may have formed during crystal growth, in response
220 to deformation, or may have resulted from a phase transition with a change in point group
221 symmetry. In the previous section, we showed that our wadsleyite samples are strictly
222 monoclinic, and a change from orthorhombic to monoclinic symmetry might well result in
223 twinning as suggested by Holl et al. (2008). In this case, at least one of the twin operations
224 should correspond to a symmetry operation of the orthorhombic space group *Imma* that is not
225 present in the monoclinic space group $I2/m$. We identified a two-fold twin axis parallel to
226 $[212]_{wds}$ and a twin plane parallel to $(122)_{wds}$ as the twin elements. None of the associated
227 symmetry operations, however, is contained in either of the space groups. Alternatively, we may
228 consider twinning to result from a phase transition from ringwoodite ($F\bar{4}3m$) to wadsleyite

(*Imma* or *I*2/*m*) given that both crystal structures share common structural modules. While a two-fold rotation around $[212]_{wds}$ or $[101]_{rwd}$ is not a symmetry operation of either of the relevant space groups, reflection on $(101)_{rwd}$ is indeed a symmetry operation of ringwoodite. Based on symmetry considerations alone, the twins in hydrous wadsleyite might have formed as a result of the phase transition from ringwoodite to wadsleyite. The pressure and temperature conditions during sample synthesis, however, are inconsistent with the formation of ringwoodite as a precursory phase to wadsleyite as they did not coincide with the stability field of ringwoodite. Twinning as a result of a phase transition with a change in point group symmetry does therefore not seem to be a likely explanation for the here-detected twins in wadsleyite.

Twinning by deformation requires substantial deviatoric stresses in combination with a structural mechanism that allows the crystal structure to fold in response to these stresses. The stress state inside the sample capsule during a multi-anvil experiment can be expected to be close to quasi-hydrostatic, in particular at high temperatures and in the presence of a hydrous fluid or melt as in our synthesis experiments. As a result, the synthesized wadsleyite crystals lack distinct deformation features such as dislocation arrays, subgrains, or oriented fractures. As discussed below, adjacent twin domains in hydrous wadsleyite mainly differ in the way the cations are ordered into the interstitial voids formed by the distorted cubic close-packing of oxygen anions, which appears to be continuous across the twin interface. The rearrangement of the cation substructures requires diffusive motion of cations rather than a directed displacement of the crystal structure as a whole. The structural relationship between adjacent twin domains therefore does not seem to be consistent with a folding of the crystal structure as expected for mechanical twinning by deformation.

This is the peer-reviewed, final accepted version for American Mineralogist, published by the Mineralogical Society of America.
The published version is subject to change. Cite as Authors (Year) Title. American Mineralogist, in press.
DOI: https://doi.org/10.2138/am-2022-8596. http://www.minsocam.org/

Twinning during crystal growth, or primary twinning (Bloss, 1971), does not require a specific structural mechanism or compliance with strict symmetry rules. Instead, growth twins tend to exploit pseudo-symmetries of a crystal structure while conserving or extending fundamental structural units across the interface between twin domains (Buerger, 1945). For wadsleyite, layers of close-packed oxygen anions parallel to $\{021\}_{wds}$ and $\{101\}_{wds}$ planes are among the most fundamental structural units (Fig. 8). Both a 180° rotation about an axis parallel to $[212]_{wds}$ and a reflection on a $(122)_{wds}$ plane map $\{021\}_{wds}$ planes onto $\{101\}_{wds}$ planes and therefore preserve layers of close-packed oxygen anions while exploiting the pseudo-symmetry of the oxygen substructure (**Supplemental Fig. S2**). As a result, layers of close-packed oxygen anions may be continuous across the composition plane while the ordering of cations into tetrahedral and octahedral voids on opposing sites of the interface is related by the twin operation. The twin law that we derived for the here-reported twins in wadsleyite is therefore consistent with growth twinning.

The twin relation can then be described by the following twin equation (e.g., Hirsch, 1977): $\{021\} + \{101\} = \{122\}$, in which one of the $\{122\}_{wds}$ planes should be one of the composition planes in orthorhombic wadsleyite (**Fig. 3**). The $\{122\}_{wds}$ planes in wadsleyite correspond to the $\{101\}_{rwd}$ planes in ringwoodite. As the mirror symmetry parallel to $\{101\}_{rwd}$ in ringwoodite is reproduced along the twin interface, the atomic structure in the vicinity of the interface between twin domains may locally resemble the spinel structure of ringwoodite.

Relation to twins in spinel and to spinelloid phases

The twin relation in wadsleyite presented here may appear similar to that of the (111) twin in $MgAl_2O_4$ spinel (e.g., Fig. 5 in Daneu et al., 2007), i.e., the spinel twin law. According to Daneu et al. (2007), (111) twins in spinel can be described by a 180° rotation of the oxygen substructure about one of the <111> axes which are perpendicular to the {111} composition planes. Despite these similarities, the twin axis and twin plane for twins in wadsleyite correspond to the cubic $<101>_{rwd}$ directions and the $\{101\}_{rwd}$ planes, respectively, i.e., not the <111> directions and {111} planes as in spinel. Instead, there might be some similarity with the iron cross law in pyrite, FeS_2 (Rečnik et al., 2016).

The twinning in wadsleyite could potentially be related to other spinelloid structures (Horiuchi et al., 1982). However, we could not detect any other phases at the composition plane nor a dense magnesium-iron silicate polymorph with a structure intermediate between olivine, ringwoodite, and wadsleyite, as for instance poirierite (Tomioka et al., 2021), wadsleyite II (Smyth and Kawamoto, 1997), or other spinelloid phases (Horiuchi et al. 1982; Davies and Akaogi, 1983). The crystal structures of two adjacent twin domains continue perfectly across the interface, i.e., the composition plane, without any significant structural mismatches or chemical changes (**Fig. 5**).

Implications

The formation of twins might have consequences for the physical properties and deformation behavior of wadsleyite in the mantle transition zone. Shear deformation experiments on wadsleyite aggregates and the analysis of the resulting microstructures indicated a dislocation creep mechanism with slip mainly on the lattice planes $(010)_{wds}$ and $\{101\}_{wds}$ (Farla et al., 2015;

Kawazoe et al., 2013; Ohuchi et al., 2014; Miyajima and Kawazoe, 2015). None of these slip planes coincides with the composition planes $(122)_{wds}$ of the here-detected twins nor do the orientations of slip planes in adjacent domains coincide at the composition plane. The resulting discontinuity of slip planes at the interface between twin domains might hinder dislocations to move across the interface. In this way, the twins in wadsleyite might impede dislocation movement and reduce the strength of deformation textures related to the affected slip systems.

Twin walls in wadsleyite may only reduce deformation rates dominated by dislocation glide. More comprehensive models for the viscoelastic behavior of wadsleyite aggregates, however, suggest that dislocation glide might be an ineffective deformation mechanism at pressures and temperatures of the mantle transition zone (Castelnau et al., 2020; Ritterbex et al., 2016) with pure climb creep being more efficient than dislocation glide except for the coldest regions of the mantle transition zone (Ritterbex et al., 2020). For climb creep, twin interfaces might act as sources of cation disorder and vacancies and promote deformation.

Depending on the frequency of twinning, the modified mobility of dislocations might have implications for the deformation of wadsleyite-bearing rocks in the mantle transition zone and the associated seismic anisotropy (Kawazoe et al., 2013; Tommasi, 2004). In addition to impairing the alignment of wadsleyite grains by deformation through dislocation glide, twins in wadsleyite will reduce the elastic anisotropy as directions with P and S wave velocity maxima in one twin domain will be mapped onto directions with intermediate wave velocities in the other twin domain (Buchen, 2018, Buchen et al., 2018). Although further research is needed to assess the potential impact of twinning on the properties of wadsleyite-bearing rocks, we anticipate a potential effect on the deformation behavior under the assumption that twinning is common in natural wadsleyite.

317 In addition to affecting physical properties, twinning in wadsleyite might have an impact
318 on the kinetics of the phase transition to ringwoodite. Our TEM observations indicate that the
319 atomic structure in the vicinity of twin boundaries resembles the structure of ringwoodite while
320 conserving the oxygen substructure across the composition plane. Because the *c* axes and [120]*
321 directions (corresponding to the *a* axis in ringwoodite) of adjacent domains meet at the
322 composition plane, the composition plane itself has the same structural unit as ringwoodite (e.g.,
323 Horiuchi et al., 1982). We present direct evidence for local structural order along the
324 composition plane in the HRTEM image of **Fig. 5a**. Boundaries between twinned domains in
325 wadsleyite might therefore act as nucleation sites for lamellae of ringwoodite. Lamellar
326 intergrowth of spinelloid phases has been observed previously in the system Ni_2SiO_4–$NiAl_2O_4$
327 (Davies and Akaogi, 1983). When wadsleyite-bearing rocks are brought into the stability field of
328 ringwoodite, for example, by downward flow in the mantle transition zone, ringwoodite lamellae
329 might preferentially nucleate along twin composition planes without need to overcome the
330 energy barrier associated with creating viable nuclei. Crystal growth of ringwoodite may then
331 proceed from the interface outwards by rearranging cations but retaining the oxygen substructure.
332 This replacement mechanism might be faster than other nucleation and growth processes.
333 However, more research is needed to understand the relation between wadsleyite twins and
334 ringwoodite nucleation and the potential impact on the kinetics of the wadsleyite–ringwoodite
335 phase transition.

336

337 **Acknowledgments**

We thank Raphael Njul for polishing wadsleyite samples and Dorothea Wiesner for preparing TEM thin foils. We further thank Tiziana Boffa Ballaran for help with single-crystal X-ray diffraction. Nobuyoshi Miyajima thanks Naotaka Tomioka and Yusuke Seto for useful discussions on diffraction intensities of monoclinic wadsleyite. The authors thank Giovanni Ferraris who kindly provided an output file of the computer program *GEMINOGRAPHY*. The constructive feedback of three reviewers helped to improve the manuscript. We acknowledge support from the German Research Foundation (DFG) in funding the FIB facility (grant INST 91/315-1 FUGG) and the TEM facility (grant INST 91/251-1 FUGG).

References cited

Bloss, F.D. (1971) Crystallography and Crystal Chemistry. New York and London (Holt, Rinehart and Winston Inc.)

Buchen, J. (2018) The Elastic Properties of Wadsleyite and Stishovite at High Pressures, PhD Thesis. Univ. of Bayreuth.

Buchen, J., Marquardt, H., Boffa Ballaran, T., Kawazoe, T., and McCammon, C. (2017) The equation of state of wadsleyite solid solutions: Constraining the effects of anisotropy and crystal chemistry. American Mineralogist, 102, 2494-2504.

Buchen, J., Marquardt, H., Speziale, S., Kawazoe, T., Ballaran, T.B., and Kurnosov, A. (2018) High-pressure single-crystal elasticity of wadsleyite and the seismic signature of water in the shallow transition zone. Earth and Planetary Science Letters, 498, 77-87.

Buerger, M.J. (1945) The genesis of twin crystals. American Mineralogist, 30, 469-482.

Castelnau, O., Derrien, K., Ritterbex, S., Carrez, P., Cordier, P., and Moulinec, H. (2020) Multiscale modeling of the effective viscoplastic behavior of Mg_2SiO_4 wadsleyite: bridging atomic and polycrystal scales. Comptes Rendus Mecanique, 348, 827-846.

Daneu, N., Recnik, A., Yamazaki, T., and Dolenec, T. (2007) Structure and chemistry of (111) twin boundaries in $MgAl_2O_4$ spinel crystals from Mogok. Physics and Chemistry of Minerals, 34, 233-247.

Davies, P.K., and Akaogi, M. (1983) Phase intergrowths in spinelloids. Nature, 305, 788-790.

Farla, R., Amulele, G., Girard, J., Miyajima, N., & Karato, S.-i. (2015). High-pressure and high-temperature deformation experiments on polycrystalline wadsleyite using the rotational Drickamer apparatus. Physics and Chemistry of Minerals, 42, 541-558.

Frost, D.J. (2008) The upper mantle and transition zone. Elements, 4, 171-176.

Grimmer, H., & Nespolo, M. (2006). Geminography: the crystallography of twins. Zeitschrift für Kristallographie - Crystalline Materials, 221, 28-50.

Hirsch, P.B. (1977) Electron Microscopy of Thin Crystals. xi, 563 pp. R. E. Krieger Pub. Co., Huntington, N.Y.

Holl, C.M., Smyth, J.R., Jacobsen, S.D., and Frost, D.J. (2008) Effects of hydration on the structure and compressibility of wadsleyite, β-(Mg_2SiO_4). American Mineralogist, 93, 598-607.

Horiuchi, H., Akaogi, M., and Sawamoto, H. (1982) Crystal structure studies on spinel-related phases, spinelloids: implications to olivine-spinel phase transformation and systematics. In: Akimoto S, Manghnani MH (eds) Advances in earth and planetary sciences 12, High-pressure research in geophysics, pp 391–403.

Horiuchi, H. and Sawamoto, H. (1981) β-Mg_2SiO_4: single-crystal X-ray diffraction study. American Mineralogist, 66, 568-575.

Inoue, T., Yurimoto, H., and Kudoh, Y. (1995) Hydrous modified spinel, $Mg_{1.75}SiH_{0.5}O_4$: a new water reservoir in the mantle transition zone. Geophysical Research Letters, 22, 117-120.

Kawazoe, T., Ohuchi, T., Nishihara, Y., Nishiyama, N., Fujino, K., & Irifune, T. (2013). Seismic anisotropy in the mantle transition zone induced by shear deformation of wadsleyite. Physics of the Earth and Planetary Interiors, 216, 91-98.

Kawazoe, T., Buchen, J., and Marquardt, H. (2015) Synthesis of large wadsleyite single crystals by solid-state recrystallization. American Mineralogist, 100, 2336-2339.

Kawazoe, T., Chaudhari, A., Smyth, J.R., and McCammon, C. (2016) Coupled substitution of Fe^{3+} and H^{+} for Si in wadsleyite: a study by polarized infrared and Mössbauer spectroscopies and single-crystal X-ray diffraction, American Mineralogist, 101, 1236-1239.

Kilaas, R. (1998) Optimal and near-optimal filters in high-resolution electron microscopy. Journal of Microscopy, 190, 45-51.

Kohlstedt, D.L., Keppler, H., and Rubie, D.C. (1996) Solubility of water in the α, β and γ phases of $(Mg,Fe)_2SiO_4$. Contributions to Mineralogy and Petrology, 123, 345-357.

Kogure, T. (2015): Geometry of electron diffraction and its calculation. Renbikyo, 50, 1-5 (in Japanese).

Kudoh, Y., and Inoue, T. (1999) Mg-vacant structural modules and dilution of the symmetry of hydrous wadsleyite, β-$Mg_{2-x}SiH_{2x}O_4$ with $0.00 \leq x \leq 0.25$. Physics and Chemistry of Minerals, 26, 382-388.

McKay, D., Moran, R.F., Dawson, D.M., Griffin, J.M., Sturniolo, S., Pickard, C.J., Berry, A.J., and Ashbrook, S.E. (2019) A picture of disorder in hydrous wadsleyite under the

combined microscope of solid-state NMR spectroscopy and ab initio random structure searching. Journal of the American Chemical Society, 141, 3024-3036.

Mitchell, D.R.G., and Schaffer, B. (2005) Scripting-customised microscopy tools for Digital Micrograph™. Ultramicroscopy, 103, 319-332.

Miyajima, N., and Kawazoe, T. (2015) Dislocation microstructures in simple-shear-deformed wadsleyite at transition-zone conditions: Weak-beam dark-field TEM characterization of dislocations on the (010) plane. American Mineralogist, 100, 2749-2752.

Momma, K. and Izumi, F. (2011) VESTA 3 for three-dimensional visualization of crystal, volumetric and morphological data. Journal of Applied Crystallography, 44, 1272-1276.

Moore, P.B. and Smith J.V. (1970) Crystal structure of β-Mg_2SiO_4: crystal-chemical and geophysical implications. Physics of the Earth and Planetary Interiors, 3, 166-177.

Nespolo, M., & Ferraris, G. (2006). The derivation of twin laws in non-merohedric twins. Application to the analysis of hybrid twins. Acta Crystallographica A, 62, 336-349.

Ohuchi, T., Fujino, K., Kawazoe, T., & Irifune, T. (2014). Crystallographic preferred orientation of wadsleyite and ringwoodite: Effects of phase transformation and water on seismic anisotropy in the mantle transition zone. Earth and Planetary Science Letters, 397, 133-144.

Price, G.D. (1983) The nature and significance of stacking-faults in wadsleyite, natural β-$(Mg, Fe)_2SiO_4$ from the Peace River Meteorite. Physics of the Earth and Planetary Interiors, 33, 137-147.

Price, G.D., Putnis, A., Agrell, S.O., and Smith, D.G.W. (1983) Wadsleyite, natural β-$(Mg,Fe)_2SiO_4$ from the Peace River Meteorite. Canadian Mineralogist, 21, 29-35.

Putnis, A. (1992) Introduction to Mineral Sciences. xx, 457 pp. Cambridge University Press, Cambridge England; New York.

Rečnik, A., Zavašnik, J., Jin, L., Čobić, A., & Daneu, N. (2016). On the origin of 'iron-cross' twins of pyrite from Mt. Katarina, Slovenia. Mineralogical Magazine, 80, 937-948. doi:10.1180/minmag.2016.080.073

Ritterbex, S., Carrez, P., and Cordier, P. (2016) Modeling dislocation glide and lattice friction in Mg_2SiO_4 wadsleyite in conditions of the Earth's transition zone. American Mineralogist, 101, 2085-2094.

-. (2020) Deformation across the mantle transition zone: a theoretical mineral physics view. Earth and Planetary Science Letters, 547, 116438.

Smyth, J.R., Bolfan-Casanova, N., Avignant, D., El-Ghozzi, M., and Hirner, S.M. (2014) Tetrahedral ferric iron in oxidized hydrous wadsleyite. American Mineralogist, 99, 458-466.

Smyth, J.R., and Kawamoto, T. (1997) Wadsleyite .2. A new high pressure hydrous phase in the peridotite-H_2O system. Earth and Planetary Science Letters, 146, E9-E16.

Smyth, J.R., Kawamoto, T., Jacobsen, S.D., Swope, R.J., Hervig, R.L., and Holloway, J.R. (1997) Crystal structure of monoclinic hydrous wadsleyite [β-$(Mg,Fe)_2SiO_4$]. American Mineralogist, 82, 270-275.

Su, D., and Zhu, Y.M. (2010) Scanning moiré fringe imaging by scanning transmission electron microscopy. Ultramicroscopy, 110, 229-233.

Tomioka, N., Bindi, L., Okuchi, T., Miyahara, M., Iitaka, T., Li, Z., Kawatsu, T., Xie, X.D., Purevjav, N., Tani, R., and Kodama, Y. (2021) Poirierite, a dense metastable polymorph of magnesium iron silicate in shocked meteorites. Communications Earth & Environment, 2.

Tommasi, A. (2004). Strain-induced seismic anisotropy of wadsleyite polycrystals and flow patterns in the mantle transition zone. Journal of Geophysical Research, 109. https://doi.org/10.1029/2004jb003158

Zhou, W.-Y., Ren, Z., Zhang, J.S., Chen, B., Hao, M., Ohuchi, T., Miyagi, L., Zhang, D., Alp, E.E., Lavina, B., and Schmandt, B. (2021) The water-Fe-pressure dependent single-crystal elastic properties of wadsleyite: Implications for the seismic anisotropy in the upper Mantle Transition Zone. Earth and Planetary Science Letters, 565, 116955.

Figure captions

Fig. 1. Polarized-light microscopic images of twins in wadsleyite between crossed polarizers (a) and in plane-polarized light (b). The thin section shown in (b) has been polished parallel to the (120) plane of domain A. As a result, the darker domain B on the right is oriented parallel to (001). Optical vibration directions (arrows) are also indicated for each domain.

Fig. 2. (a) Secondary electron image during the micro-sampling of a TEM lamella across a twin interface detected with polarized light microscopy (Fig. 1b). (b, c) Optical microscopy images of the TEM lamella.

Fig. 3. (a) Dark-field TEM image (with **g** = 244) of a twinned wadsleyite grain. The composition plane runs along the diagonal direction of the FIB-sampling TEM foil. (b) The SAED pattern of the [$2\bar{1}0$] zone axis from an area including the composition plane and (c) the corresponding PsSAED pattern. The precession angle is 3°. Note how the 244 diffraction spots (and higher orders) are split perpendicular to the composition plane. **The indexing of host domain (A) and twin domain (B) in the diffraction pattern (b)**.

Fig. 4. (a) Bright-field TEM image and (b) LACBED pattern across a composition plane viewed along the [$2\bar{1}0$] zone axis of wadsleyite. The convergent angle is more than 100 mrad (~ 5°). (c) The composition plane was moved off-center on the LACBED pattern for better visualization.

Fig. 5. (a) Filtered high-resolution TEM, (b) high-resolution bright-field STEM, and (c) bright-field scanning moiré fringe (SMF) imaging of a composition plane viewed along the [$2\bar{1}0$] zone axis of wadsleyite. The directions of moiré fringes indicate a clear discontinuity across the interface between two domains. Note that in (a) the foil thickness decreases towards the right-

478 hand side. The SMF image in (c) was taken under 66 times lower electron dose than that of the
479 high-resolution bright-field STEM image in (b).

480 Fig. 6. SAED patterns of the [001] zone axis of wadsleyite. In (a) there is no detectable intensity
481 for $hk0$ reflections with $h,k = 2n + 1$, e.g. at the expected position of the 110_m reflection (red
482 circle). In (b) the 110_m reflection becomes visible in a systematic tilt condition along the [110]*
483 (and [120]*) direction.

484 Fig. 7. (a) A HOLZ pattern of the [001] zone axis of wadsleyite using a camera length of 340
485 mm in a Philips CM20FEG TEM. The observed intensity distributions along the a^* axis (red
486 ellipses) are incompatible with a mirror plane (m) perpendicular to the a axis. (b) Simulated
487 HOLZ pattern for wadsleyite with orthorhombic symmetry, using the EDA software (courtesy of
488 Prof. Kogure). (c) For comparison, a HOLZ pattern of the $[\bar{1}10]$ zone axis of olivine, space
489 group *Pbnm*, i.e., $P2_1/b\ 2_1/n\ 2_1/m$, recorded with the same TEM instrument. The mirror
490 symmetry of olivine perpendicular to the **c** axis is clearly reflected in the HOLZ pattern.

491 Fig. 8. Depiction of the crystal structures of wadsleyite (a,c) and ringwoodite (b,d). Red spheres
492 show oxygen anions; blue tetrahedra host silicon cations; green octahedra host magnesium and
493 iron cations. The axis systems and crystal structures are drawn to preserve the orientational
494 relationship between both crystal structures. In (a) and (b), orange planes indicate the orientation
495 of close-packed layers of oxygen anions. In (c) and (d), the crystal structures of wadsleyite and
496 ringwoodite are projected along the $(\bar{1}22)_{wds}$ and $(011)_{rwd}$ planes, respectively, to highlight
497 structural similarities. The orientation of twin axes and twin planes with respect to the axis
498 systems of both crystal structures is indicated in red. Graphics were created with *VESTA*
499 (Momma and Izumi, 2011).

Table 1. Unit cell parameters of a twinned wadsleyite crystal

Space-group type	*Imma*	*I*2/*m*
a (Å)	5.6936(4)	5.6939(2)
b (Å)	11.5067(3)	11.5067(2)
c (Å)	8.2676(3)	8.2678(2)
V (Å^3)	541.65(4)	541.68(3)
β (°)	90	90.030(3)
b/*a*	2.0210(2)	2.0209(1)
N[a]	33	33

Note: Standard deviations on the last digit are given in parentheses.

[a] Number of reflections centered on a four-circle diffractometer.

This is the peer-reviewed, final accepted version for American Mineralogist, published by the Mineralogical Society of America.
The published version is subject to change. Cite as Authors (Year) Title. American Mineralogist, in press.
DOI: https://doi.org/10.2138/am-2022-8596. http://www.minsocam.org/

501 **Figures_ms8596_Revision 2**

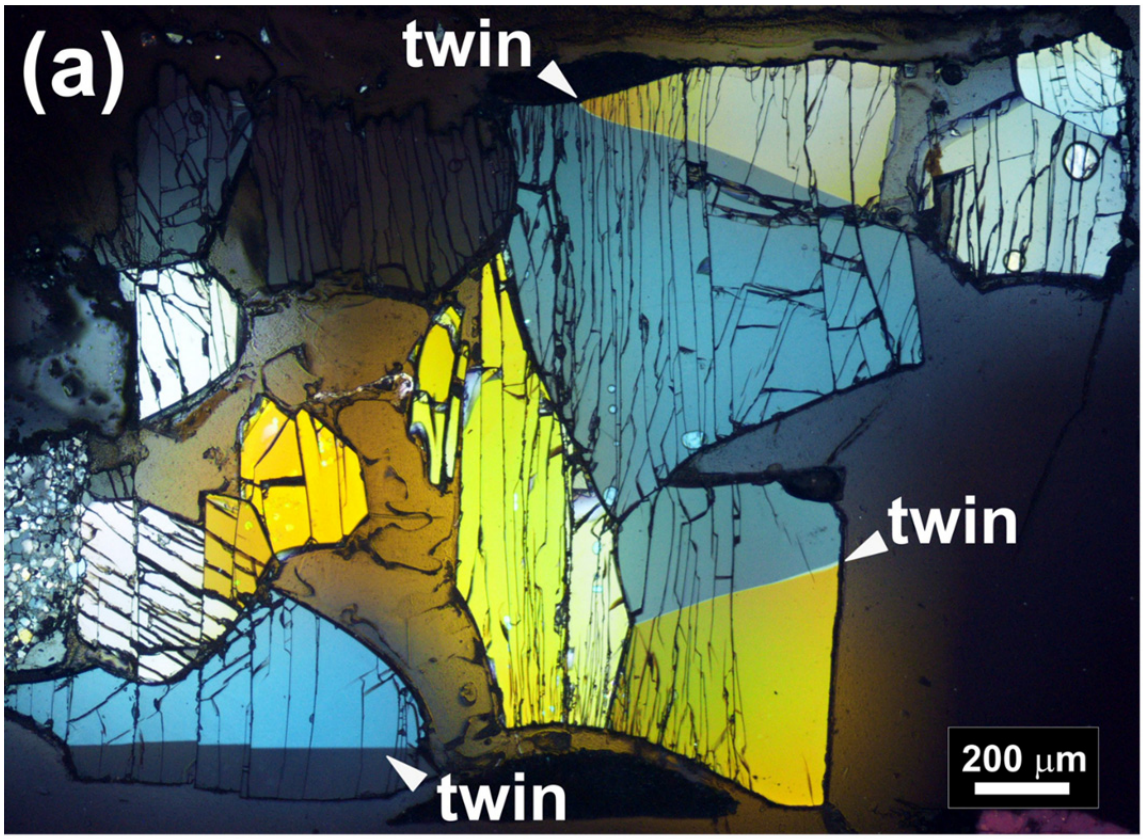

502 Fig. 1a

This is the peer-reviewed, final accepted version for American Mineralogist, published by the Mineralogical Society of America.
The published version is subject to change. Cite as Authors (Year) Title. American Mineralogist, in press.
DOI: https://doi.org/10.2138/am-2022-8596. http://www.minsocam.org/

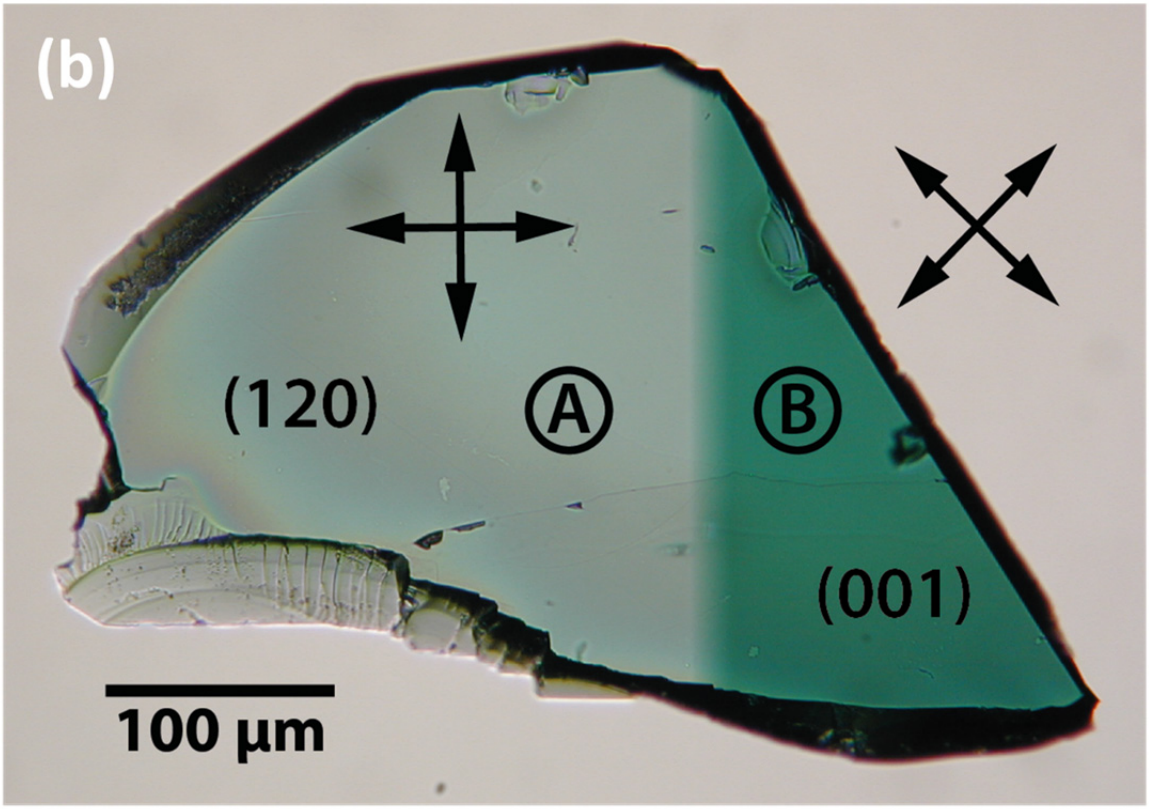

Fig. 1b

Fig. 1. Polarized-light microscopic images of twins in wadsleyite between crossed polarizers (a) and in plane-polarized light (b). The thin section shown in (b) has been polished parallel to the (120) plane of domain A. As a result, the darker domain B on the right is oriented parallel to (001). Optical vibration directions (arrows) are also indicated for each domain.

This is the peer-reviewed, final accepted version for American Mineralogist, published by the Mineralogical Society of America.
The published version is subject to change. Cite as Authors (Year) Title. American Mineralogist, in press.
DOI: https://doi.org/10.2138/am-2022-8596. http://www.minsocam.org/

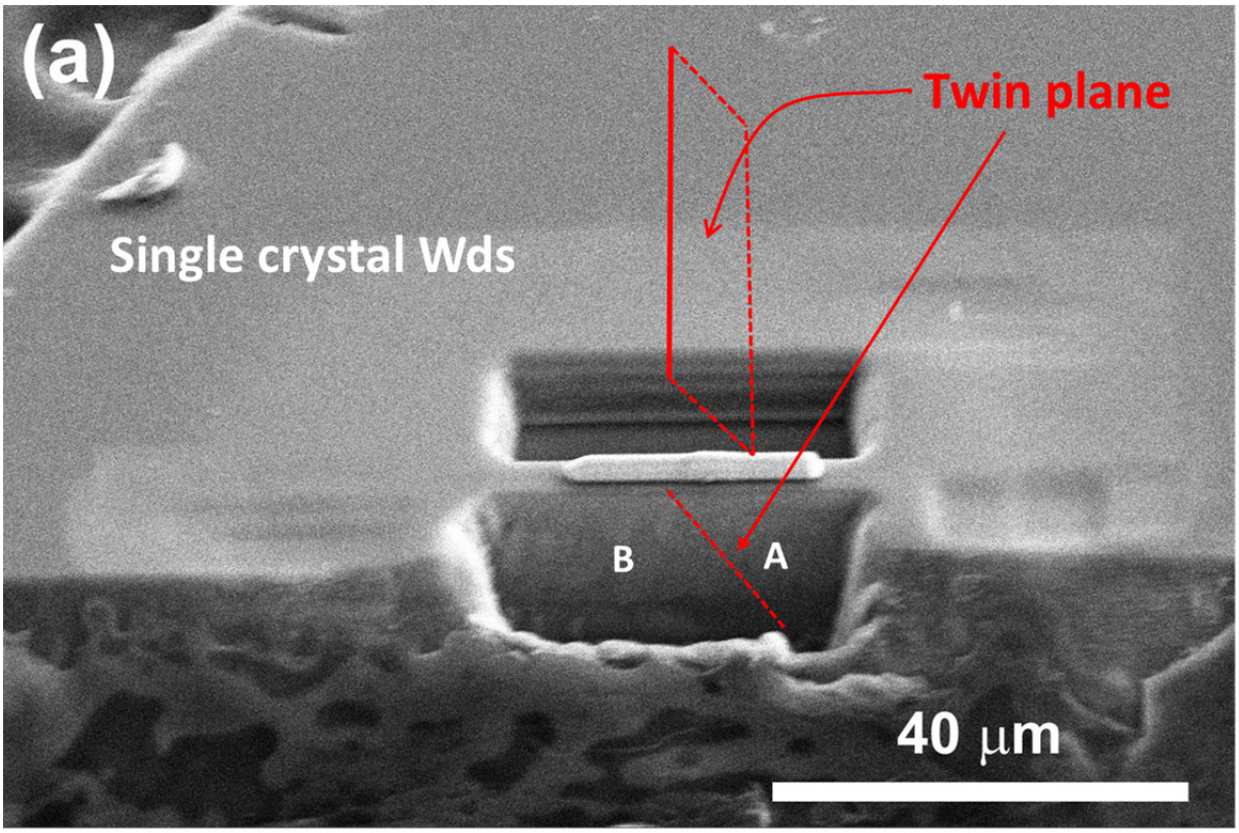

Fig. 2a

509

This is the peer-reviewed, final accepted version for American Mineralogist, published by the Mineralogical Society of America.
The published version is subject to change. Cite as Authors (Year) Title. American Mineralogist, in press.
DOI: https://doi.org/10.2138/am-2022-8596. http://www.minsocam.org/

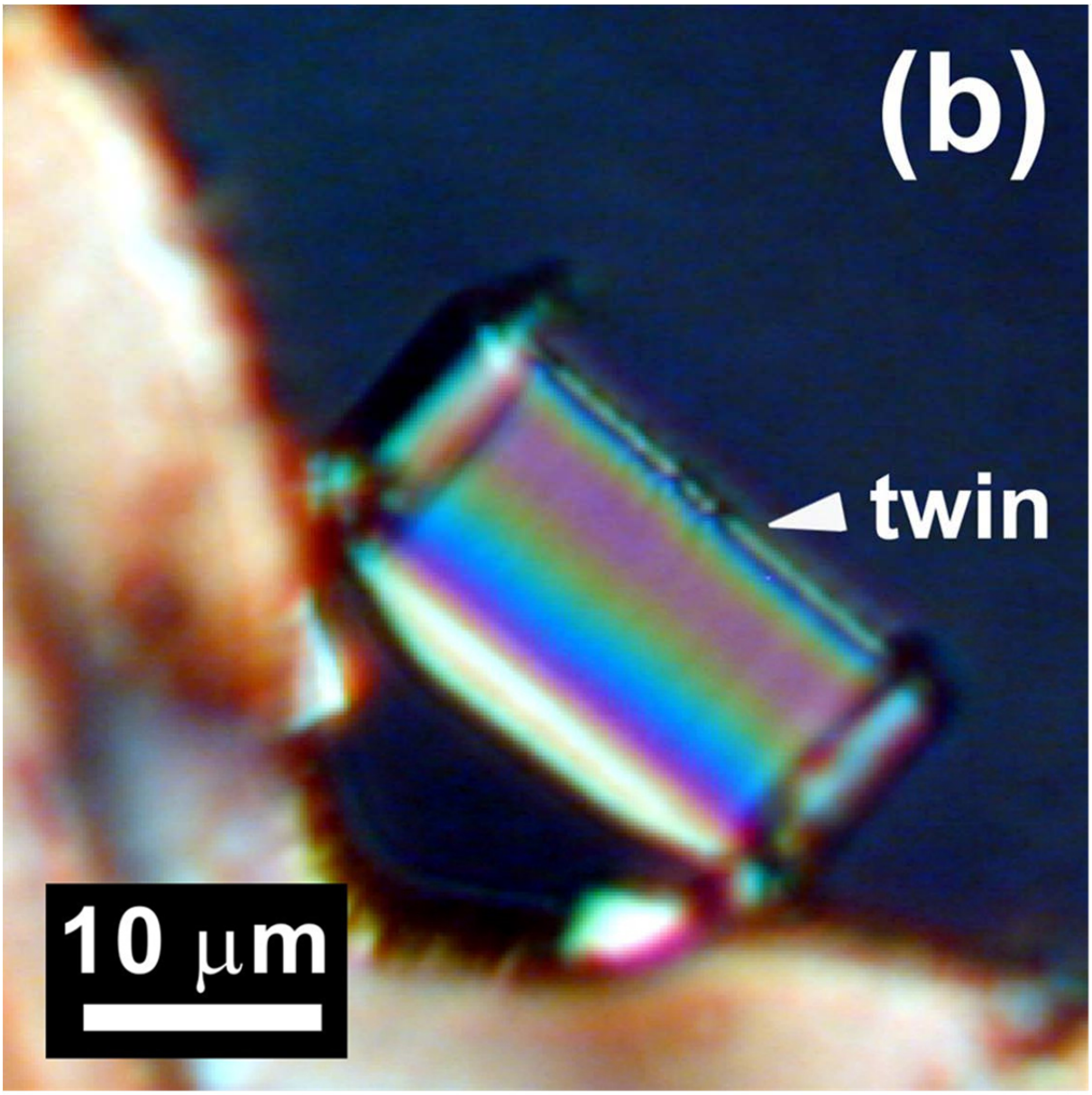

Fig. 2b

510

511

This is the peer-reviewed, final accepted version for American Mineralogist, published by the Mineralogical Society of America.
The published version is subject to change. Cite as Authors (Year) Title. American Mineralogist, in press.
DOI: https://doi.org/10.2138/am-2022-8596. http://www.minsocam.org/

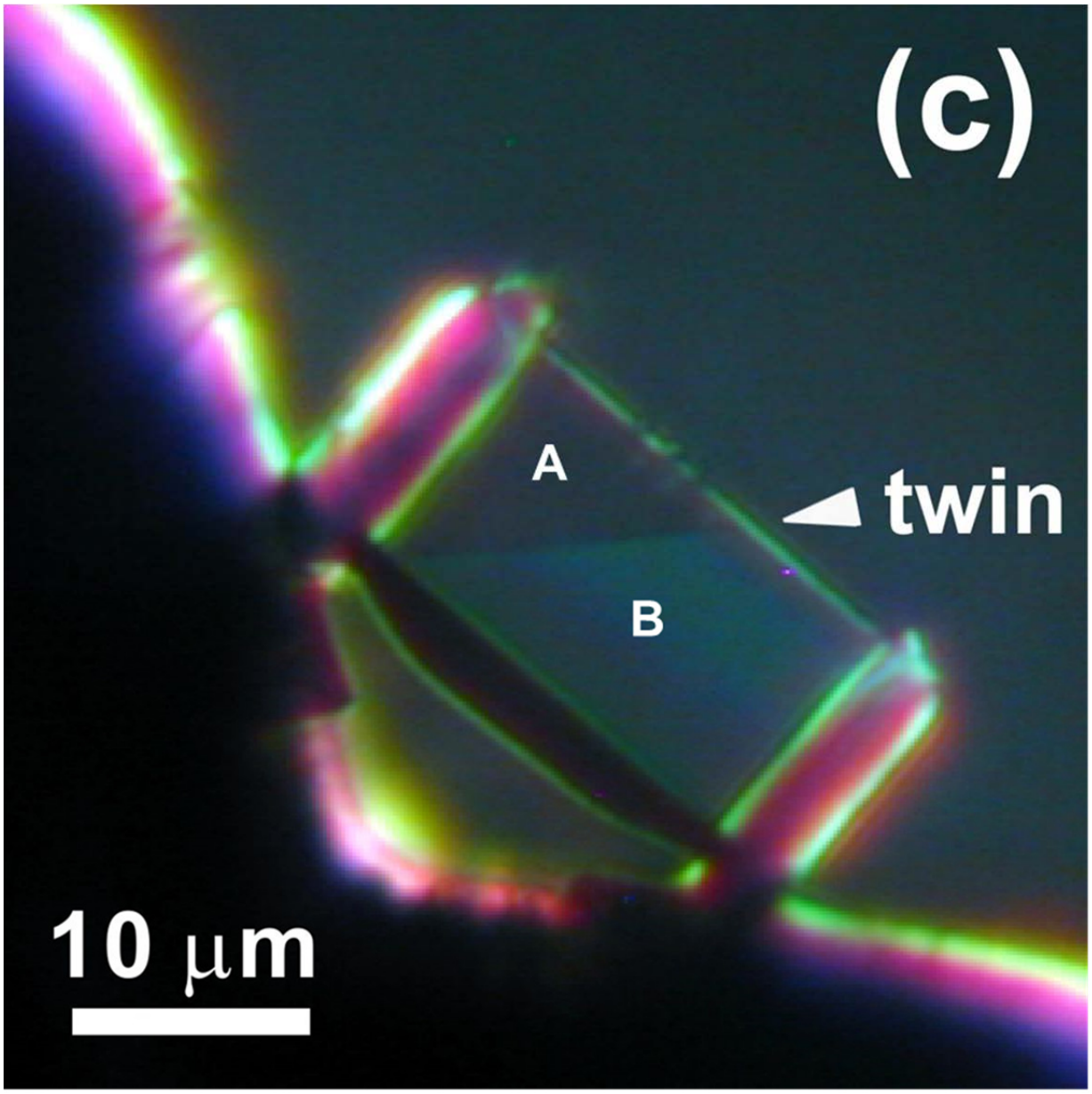

Fig. 2c

Fig. 2. (a) Secondary electron image during the micro-sampling of a TEM lamella across a twin interface detected with polarized light microscopy (Fig. 1b). (b, c) Optical microscopy images of the TEM lamella.

This is the peer-reviewed, final accepted version for American Mineralogist, published by the Mineralogical Society of America.
The published version is subject to change. Cite as Authors (Year) Title. American Mineralogist, in press.
DOI: https://doi.org/10.2138/am-2022-8596. http://www.minsocam.org/

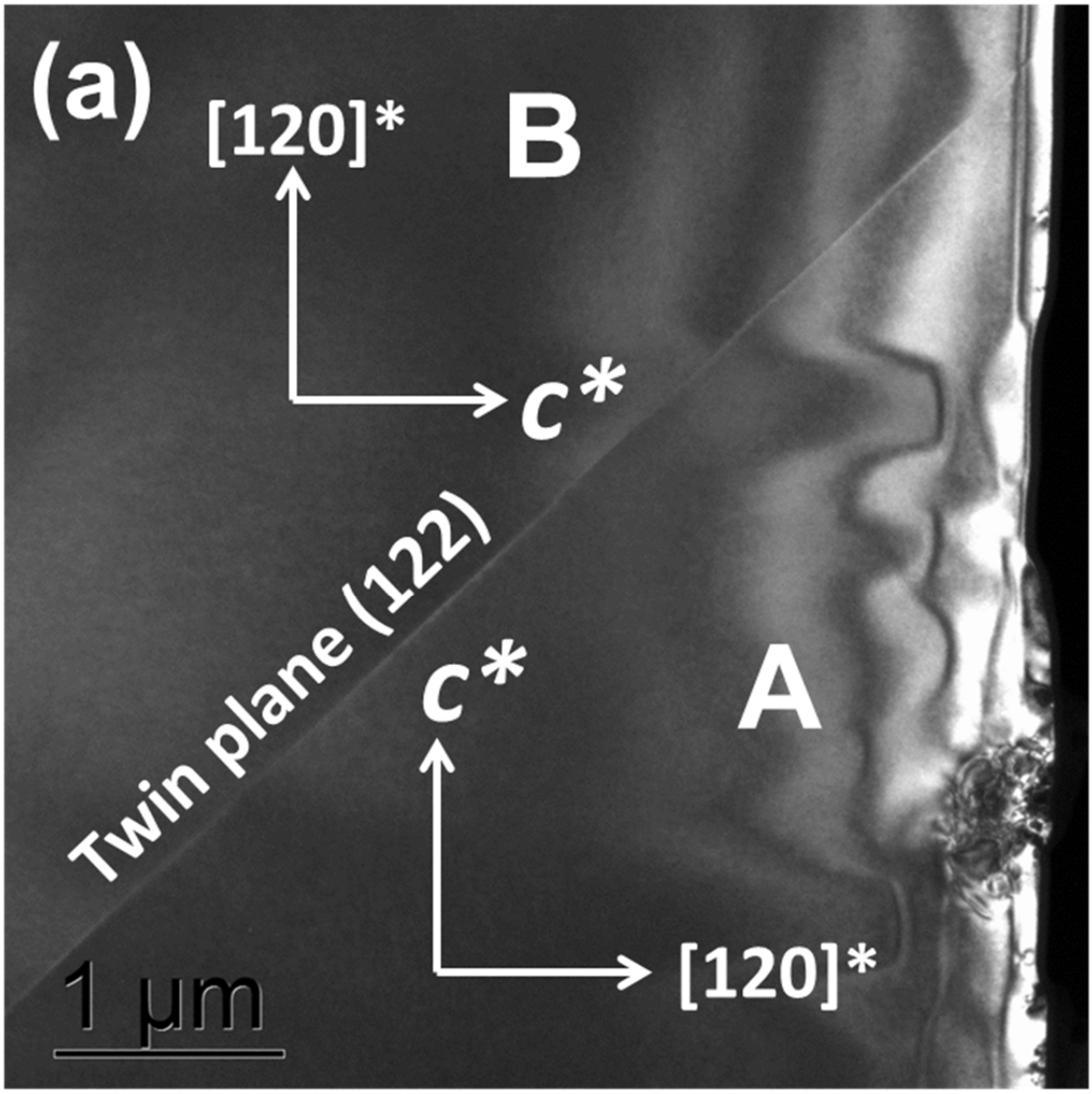

Fig. 3a

517

This is the peer-reviewed, final accepted version for American Mineralogist, published by the Mineralogical Society of America.
The published version is subject to change. Cite as Authors (Year) Title. American Mineralogist, in press.
DOI: https://doi.org/10.2138/am-2022-8596. http://www.minsocam.org/

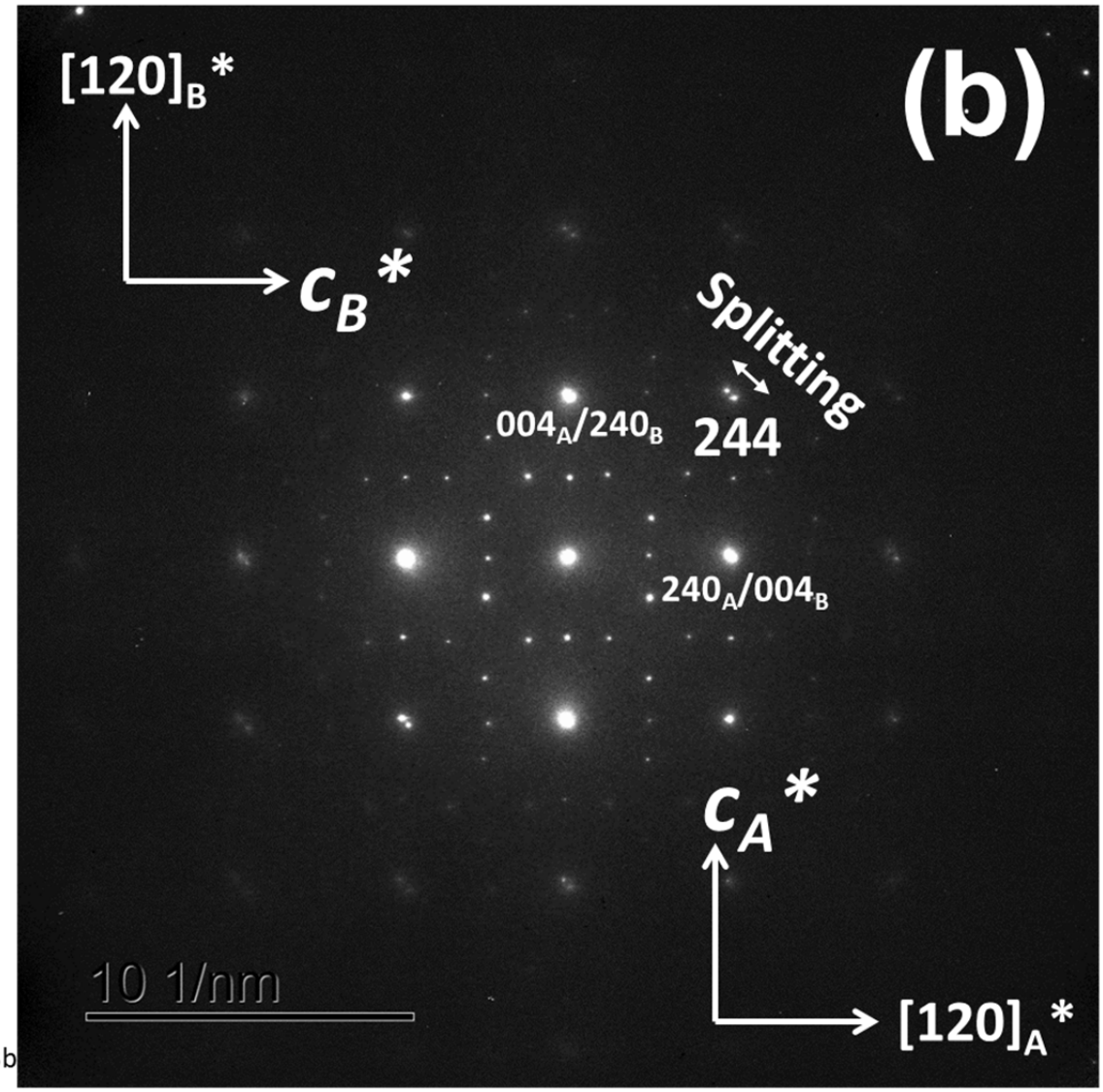

Fig. 3b

518

This is the peer-reviewed, final accepted version for American Mineralogist, published by the Mineralogical Society of America.
The published version is subject to change. Cite as Authors (Year) Title. American Mineralogist, in press.
DOI: https://doi.org/10.2138/am-2022-8596. http://www.minsocam.org/

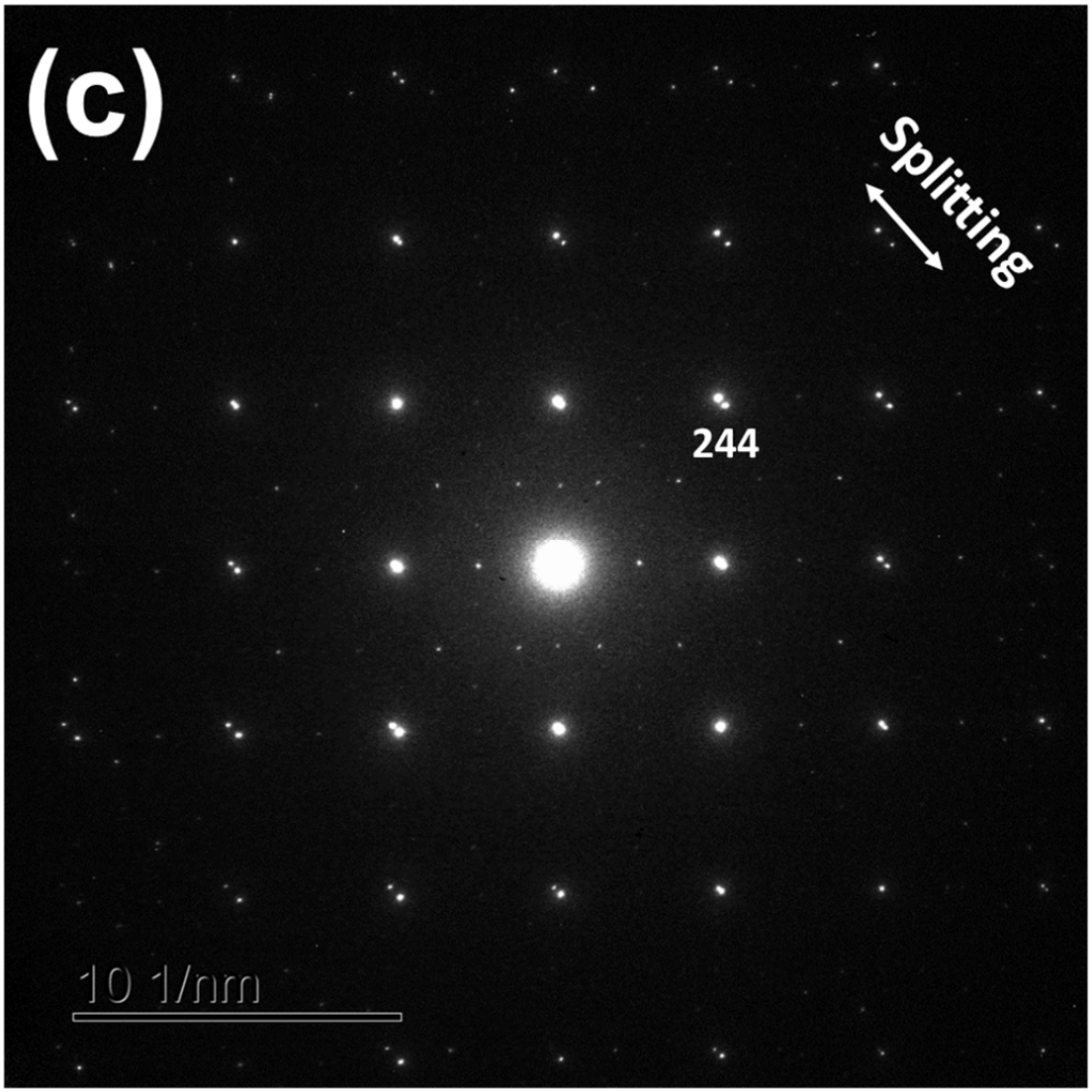

Fig. 3c

Fig. 3. (a) Dark-field TEM image (with **g** = 244) of a twinned wadsleyite grain. The composition plane runs along the diagonal direction of the FIB-sampling TEM foil. (b) The SAED pattern of the $[2\bar{1}0]$ zone axis from an area including the composition plane and (c) the corresponding PsSAED pattern. The precession angle is 3°. Note how the 244 diffraction spots (and higher orders) are split perpendicular to the composition plane. **The indexing of host domain (A) and twin domain (B) in the diffraction pattern (b)**.

This is the peer-reviewed, final accepted version for American Mineralogist, published by the Mineralogical Society of America.
The published version is subject to change. Cite as Authors (Year) Title. American Mineralogist, in press.
DOI: https://doi.org/10.2138/am-2022-8596. http://www.minsocam.org/

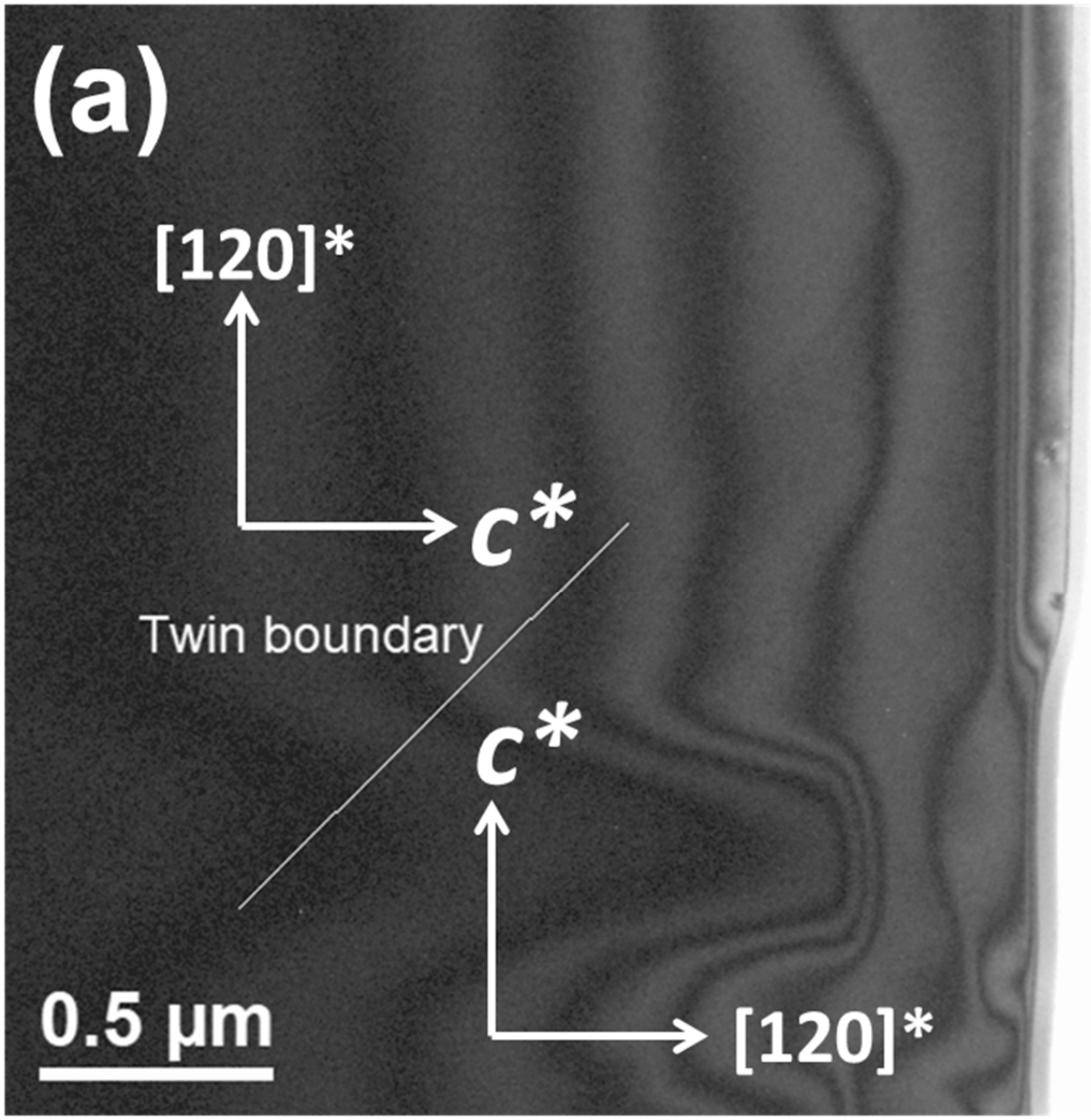

Fig. 4a

527

528

This is the peer-reviewed, final accepted version for American Mineralogist, published by the Mineralogical Society of America.
The published version is subject to change. Cite as Authors (Year) Title. American Mineralogist, in press.
DOI: https://doi.org/10.2138/am-2022-8596. http://www.minsocam.org/

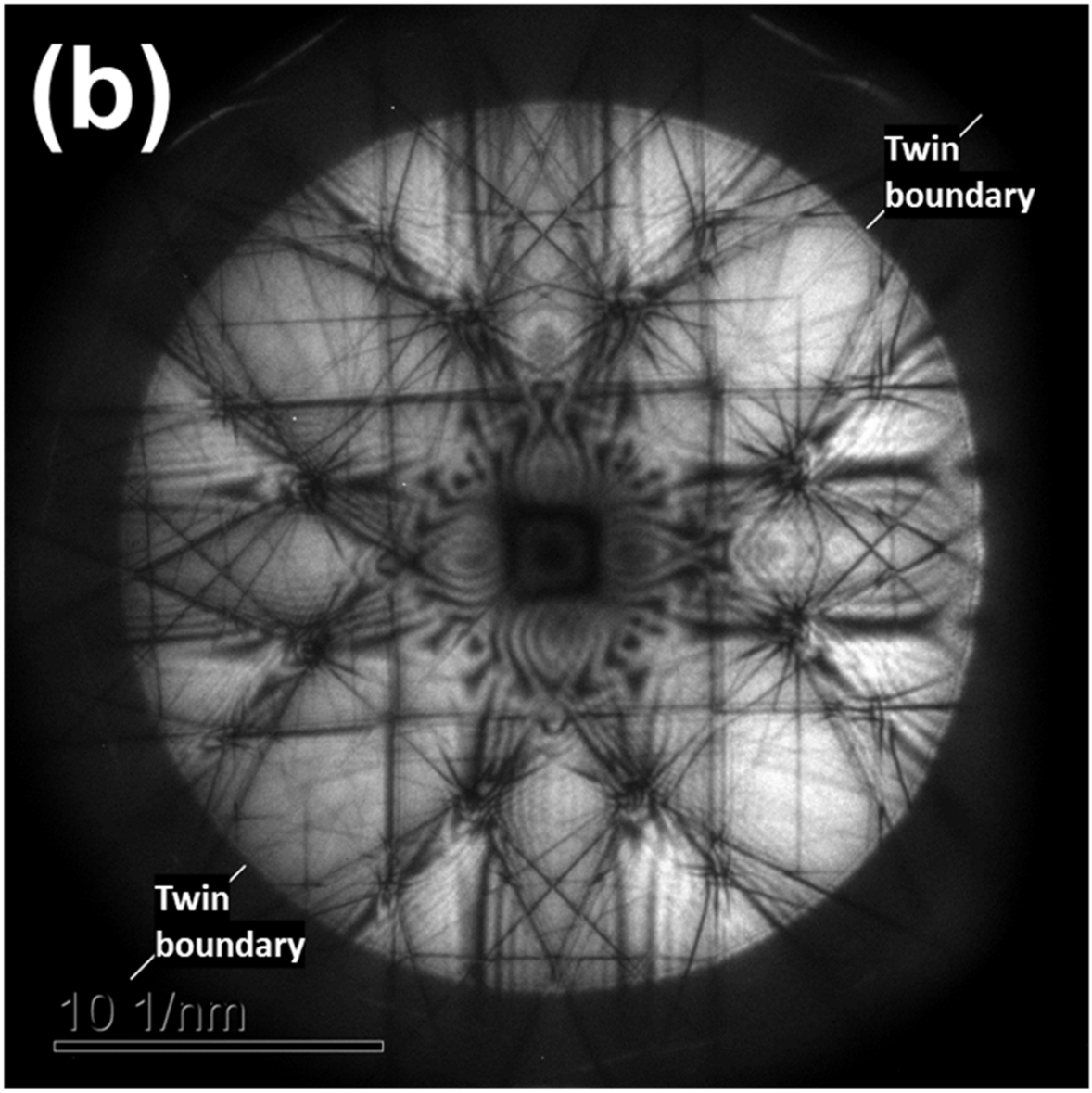

Fig. 4b

529

530

This is the peer-reviewed, final accepted version for American Mineralogist, published by the Mineralogical Society of America.
The published version is subject to change. Cite as Authors (Year) Title. American Mineralogist, in press.
DOI: https://doi.org/10.2138/am-2022-8596. http://www.minsocam.org/

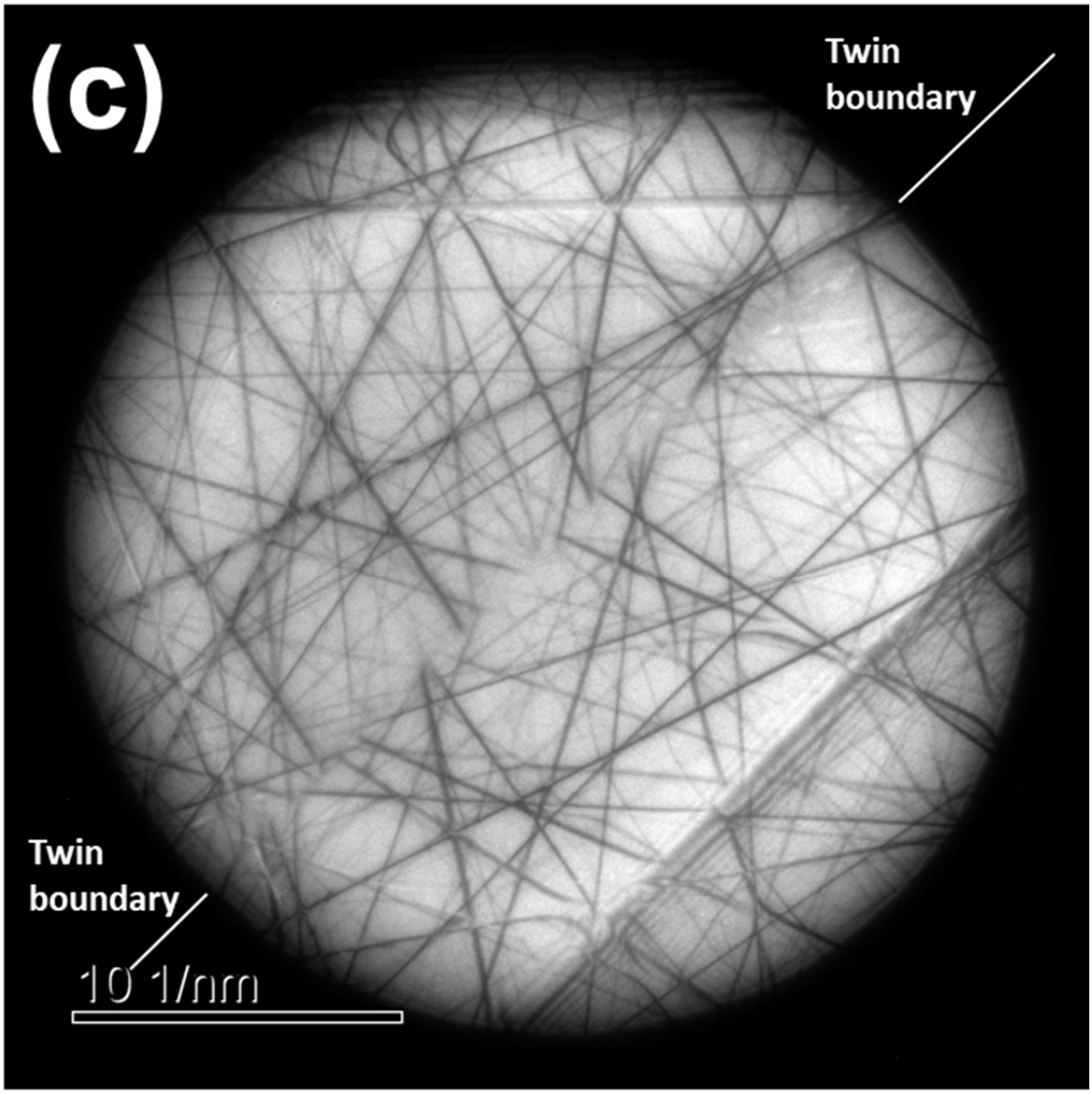

Fig. 4c

Fig. 4. (a) Bright-field TEM image and (b) LACBED pattern across a composition plane viewed along the [$2\bar{1}0$] zone axis of wadsleyite. The convergent angle is more than 100 mrad (~ 5°). (c) The composition plane was moved off-center on the LACBED pattern for better visualization.

This is the peer-reviewed, final accepted version for American Mineralogist, published by the Mineralogical Society of America.
The published version is subject to change. Cite as Authors (Year) Title. American Mineralogist, in press.
DOI: https://doi.org/10.2138/am-2022-8596. http://www.minsocam.org/

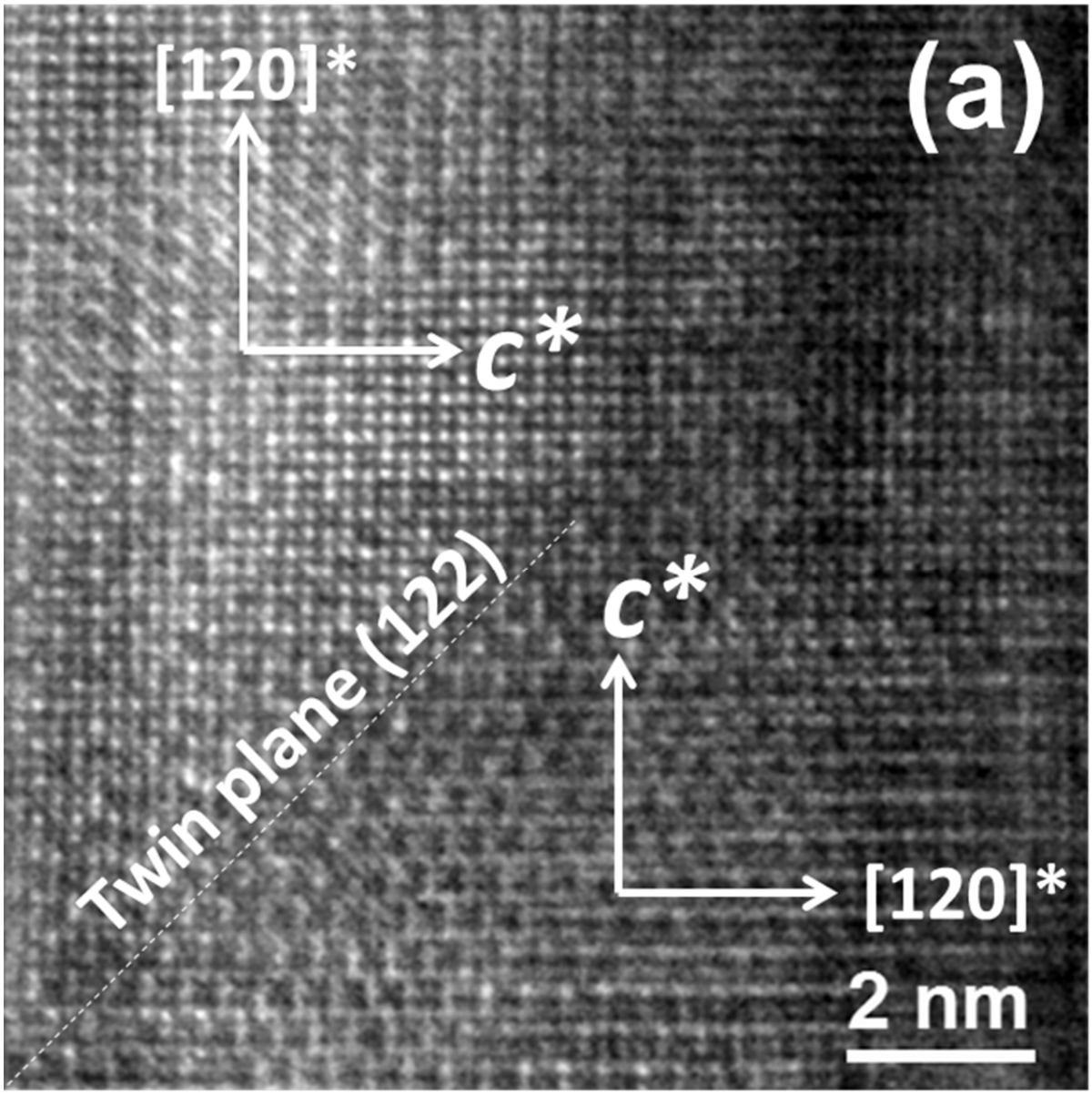

Fig. 5a

536
537

This is the peer-reviewed, final accepted version for American Mineralogist, published by the Mineralogical Society of America.
The published version is subject to change. Cite as Authors (Year) Title. American Mineralogist, in press.
DOI: https://doi.org/10.2138/am-2022-8596. http://www.minsocam.org/

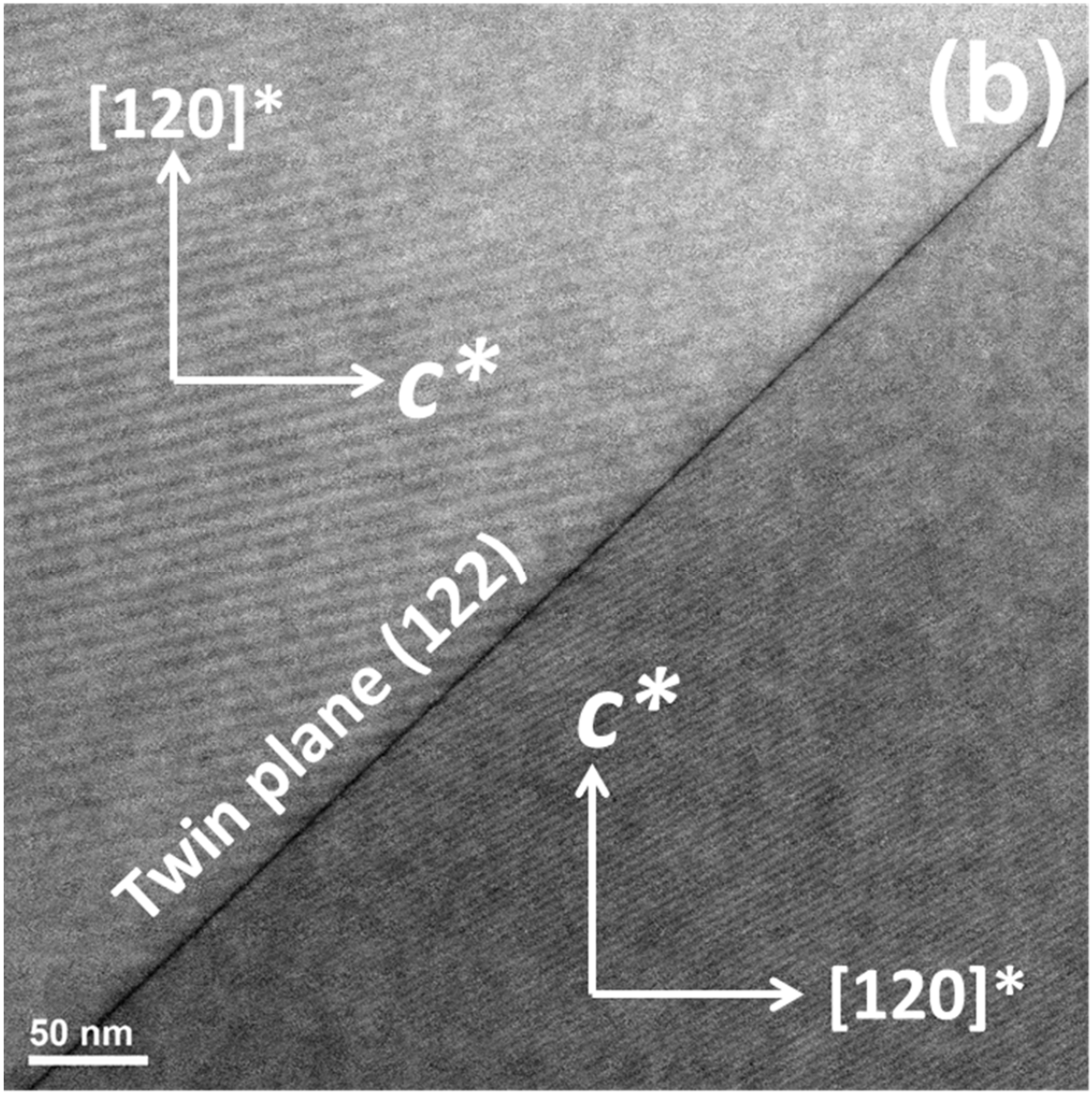

Fig. 5b

538

539

This is the peer-reviewed, final accepted version for American Mineralogist, published by the Mineralogical Society of America.
The published version is subject to change. Cite as Authors (Year) Title. American Mineralogist, in press.
DOI: https://doi.org/10.2138/am-2022-8596. http://www.minsocam.org/

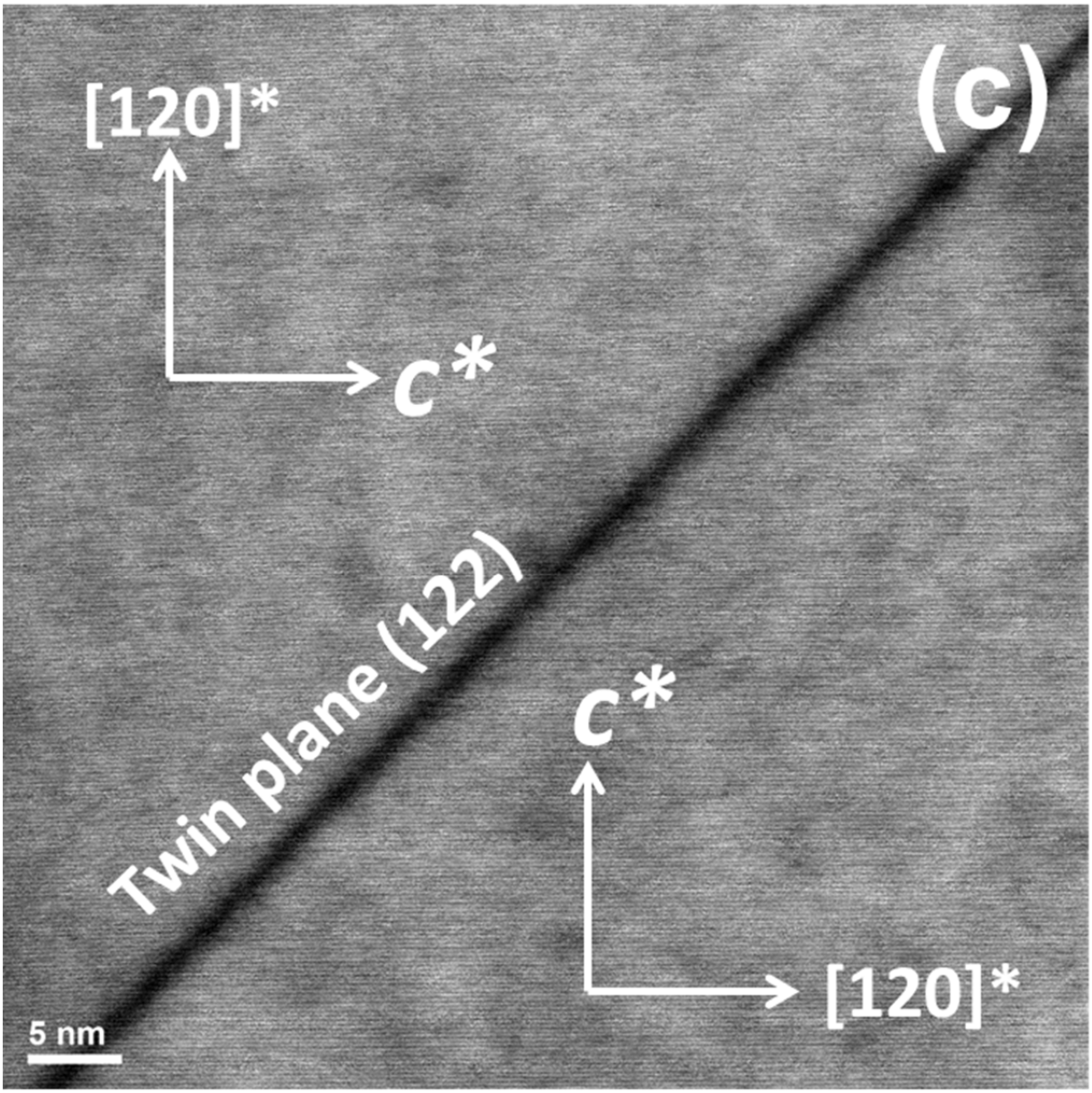

Fig. 5c

Fig. 5. (a) Filtered high-resolution TEM, (b) high-resolution bright-field STEM, and (c) bright-field scanning moiré fringe (SMF) imaging of a composition plane viewed along the [$2\bar{1}0$] zone axis of wadsleyite. The directions of moiré fringes indicate a clear discontinuity across the interface between two domains. Note that in (a) the foil thickness decreases towards the right-

545 hand side. The SMF image in (c) was taken under 66 times lower electron dose than that of the
546 high-resolution bright-field STEM image in (b).

547

This is the peer-reviewed, final accepted version for American Mineralogist, published by the Mineralogical Society of America.
The published version is subject to change. Cite as Authors (Year) Title. American Mineralogist, in press.
DOI: https://doi.org/10.2138/am-2022-8596. http://www.minsocam.org/

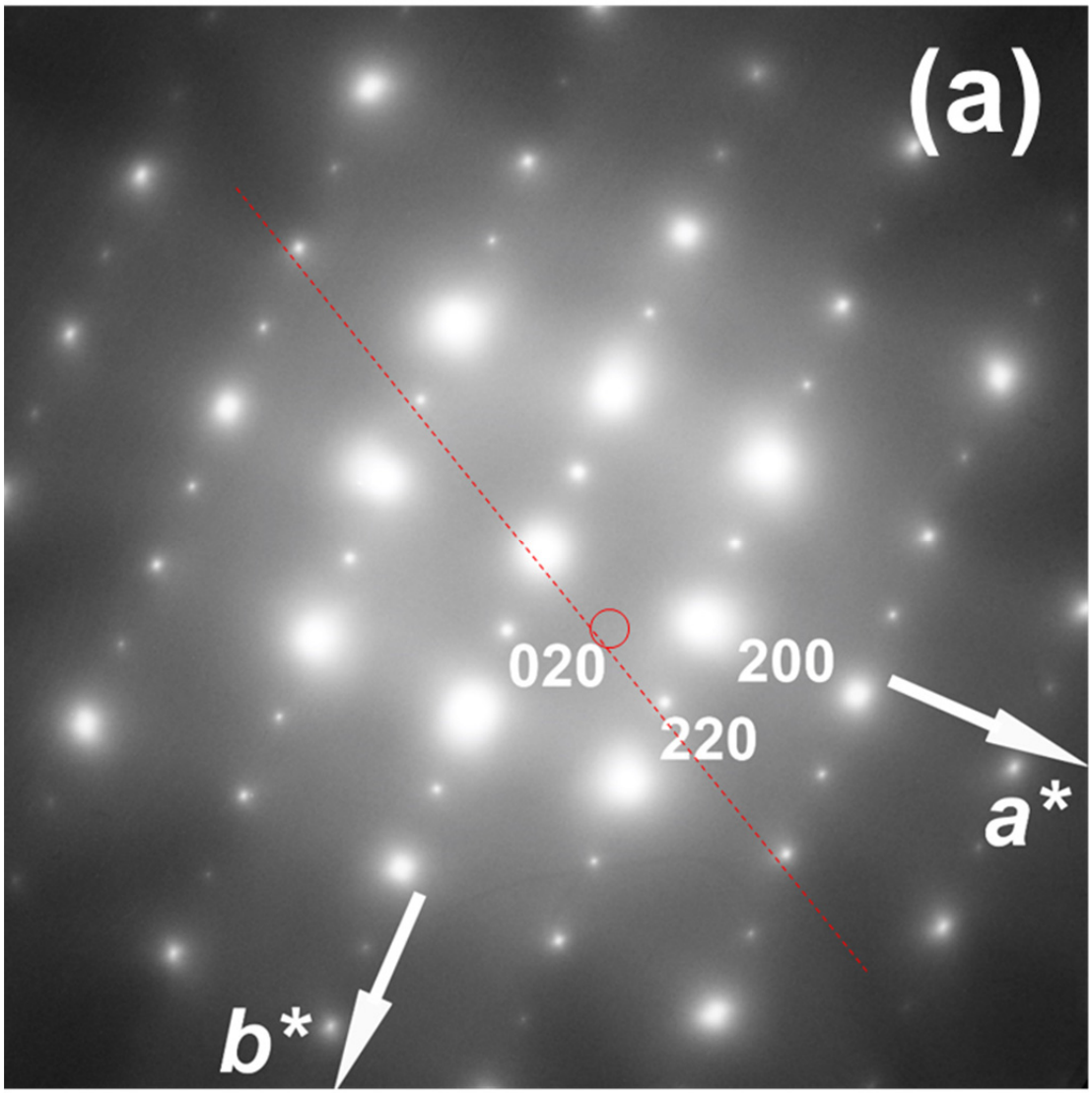

Fig. 6a

548

549

550

This is the peer-reviewed, final accepted version for American Mineralogist, published by the Mineralogical Society of America.
The published version is subject to change. Cite as Authors (Year) Title. American Mineralogist, in press.
DOI: https://doi.org/10.2138/am-2022-8596. http://www.minsocam.org/

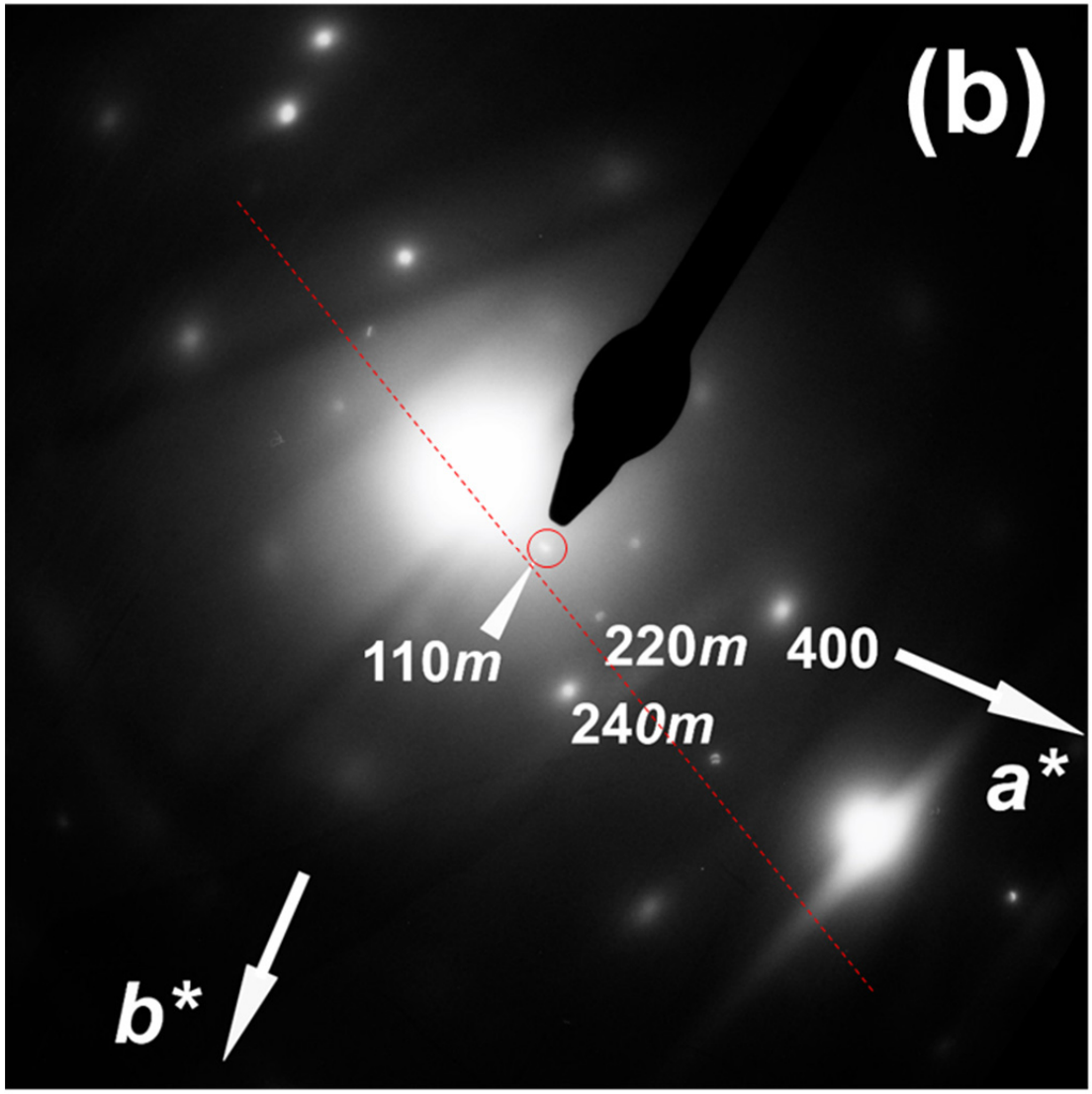

Fig. 6b

Fig. 6. SAED patterns of the [001] zone axis of wadsleyite. In (a) there is no detectable intensity for $hk0$ reflections with $h,k = 2n + 1$, e.g. at the expected position of the 110_m reflection (red circle). In (b) the 110_m reflection becomes visible in a systematic tilt condition along the [110]* (and [120]*) direction.

This is the peer-reviewed, final accepted version for American Mineralogist, published by the Mineralogical Society of America.
The published version is subject to change. Cite as Authors (Year) Title. American Mineralogist, in press.
DOI: https://doi.org/10.2138/am-2022-8596. http://www.minsocam.org/

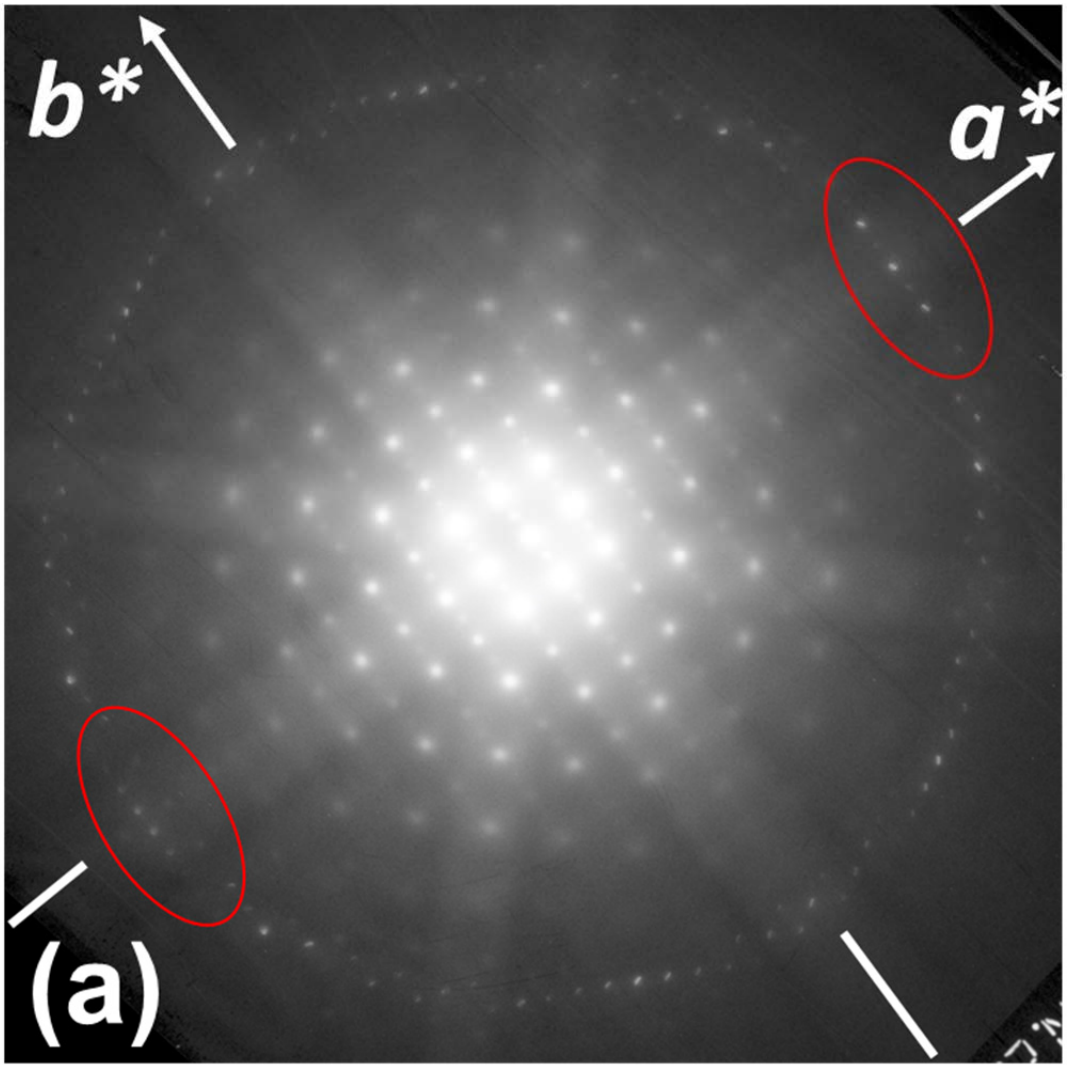

Fig. 7a

557

558

This is the peer-reviewed, final accepted version for American Mineralogist, published by the Mineralogical Society of America.
The published version is subject to change. Cite as Authors (Year) Title. American Mineralogist, in press.
DOI: https://doi.org/10.2138/am-2022-8596. http://www.minsocam.org/

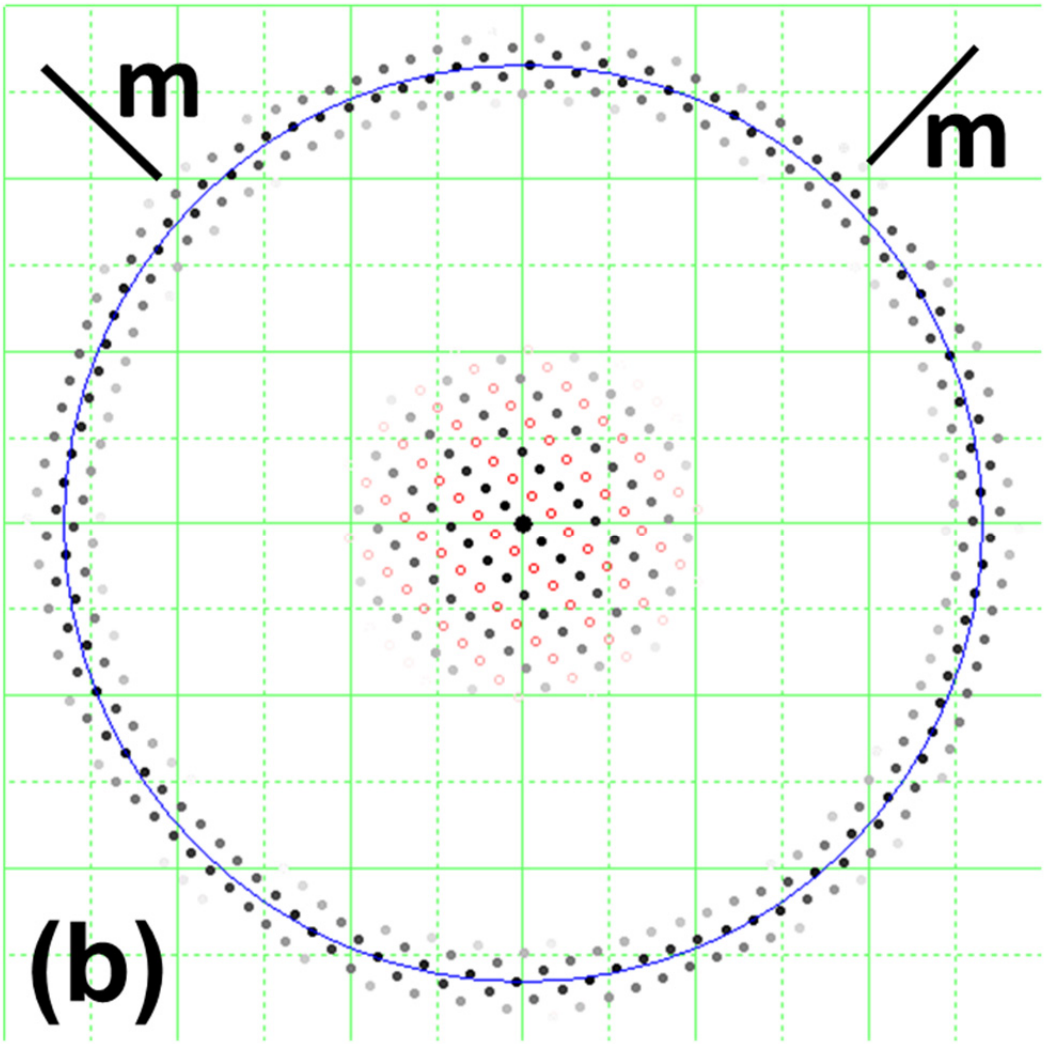

Fig. 7b

559

560

This is the peer-reviewed, final accepted version for American Mineralogist, published by the Mineralogical Society of America.
The published version is subject to change. Cite as Authors (Year) Title. American Mineralogist, in press.
DOI: https://doi.org/10.2138/am-2022-8596. http://www.minsocam.org/

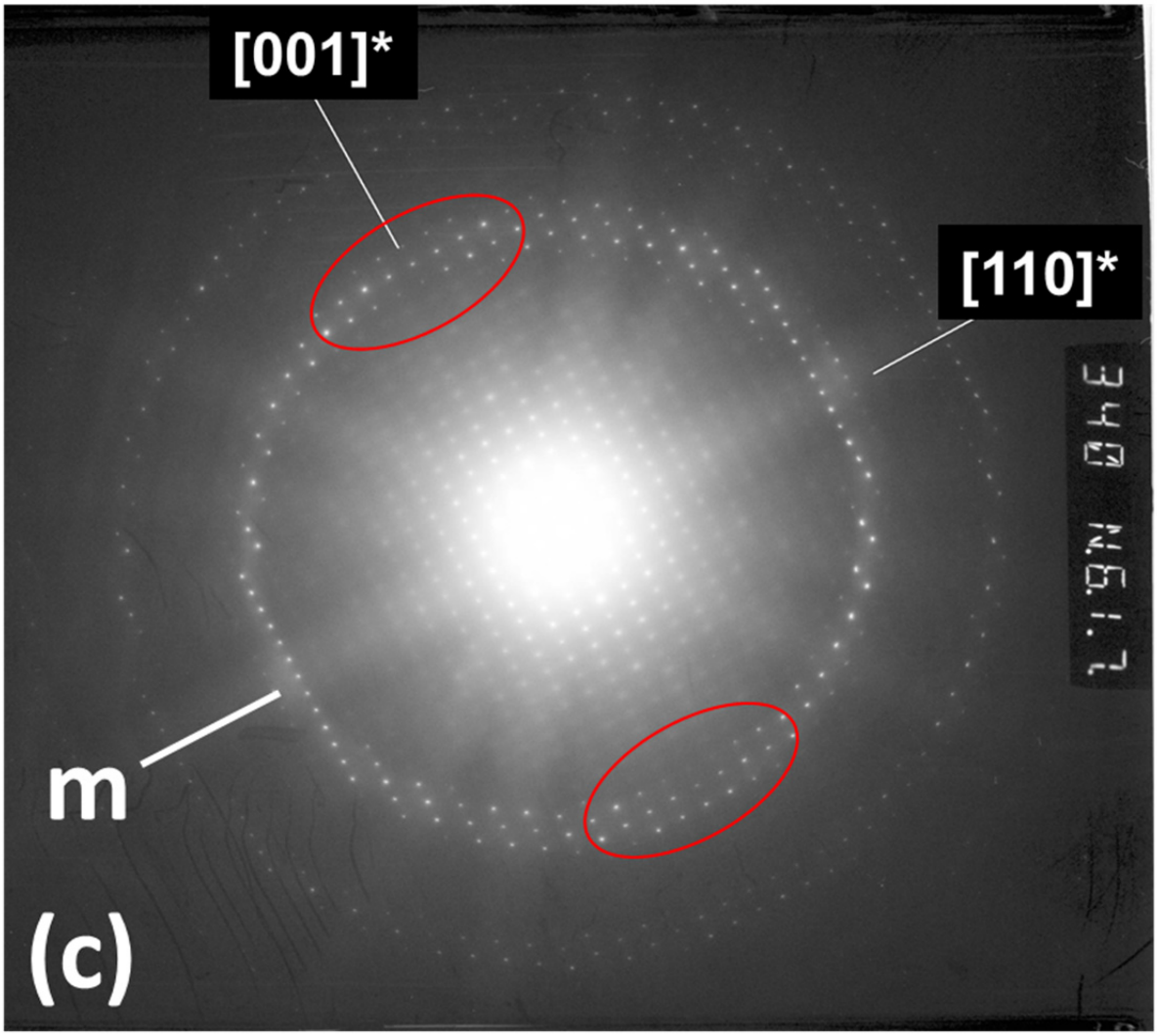

Fig. 7c

561

562 Fig. 7. (a) A HOLZ pattern of the [001] zone axis of wadsleyite using a camera length of 340
563 mm in a Philips CM20FEG TEM. The observed intensity distributions along the a^* axis (red
564 ellipses) are incompatible with a mirror plane (m) perpendicular to the a axis. (b) Simulated
565 HOLZ pattern for wadsleyite with orthorhombic symmetry, using the EDA software (courtesy of
566 Prof. Kogure). (c) For comparison, a HOLZ pattern of the $[\bar{1}10]$ zone axis of olivine, space
567 group *Pbnm*, i.e., $P2_1/b\ 2_1/n\ 2_1/m$, recorded with the same TEM instrument. The mirror
568 symmetry of olivine perpendicular to the **c** axis is clearly reflected in the HOLZ pattern.

This is the peer-reviewed, final accepted version for American Mineralogist, published by the Mineralogical Society of America.
The published version is subject to change. Cite as Authors (Year) Title. American Mineralogist, in press.
DOI: https://doi.org/10.2138/am-2022-8596. http://www.minsocam.org/

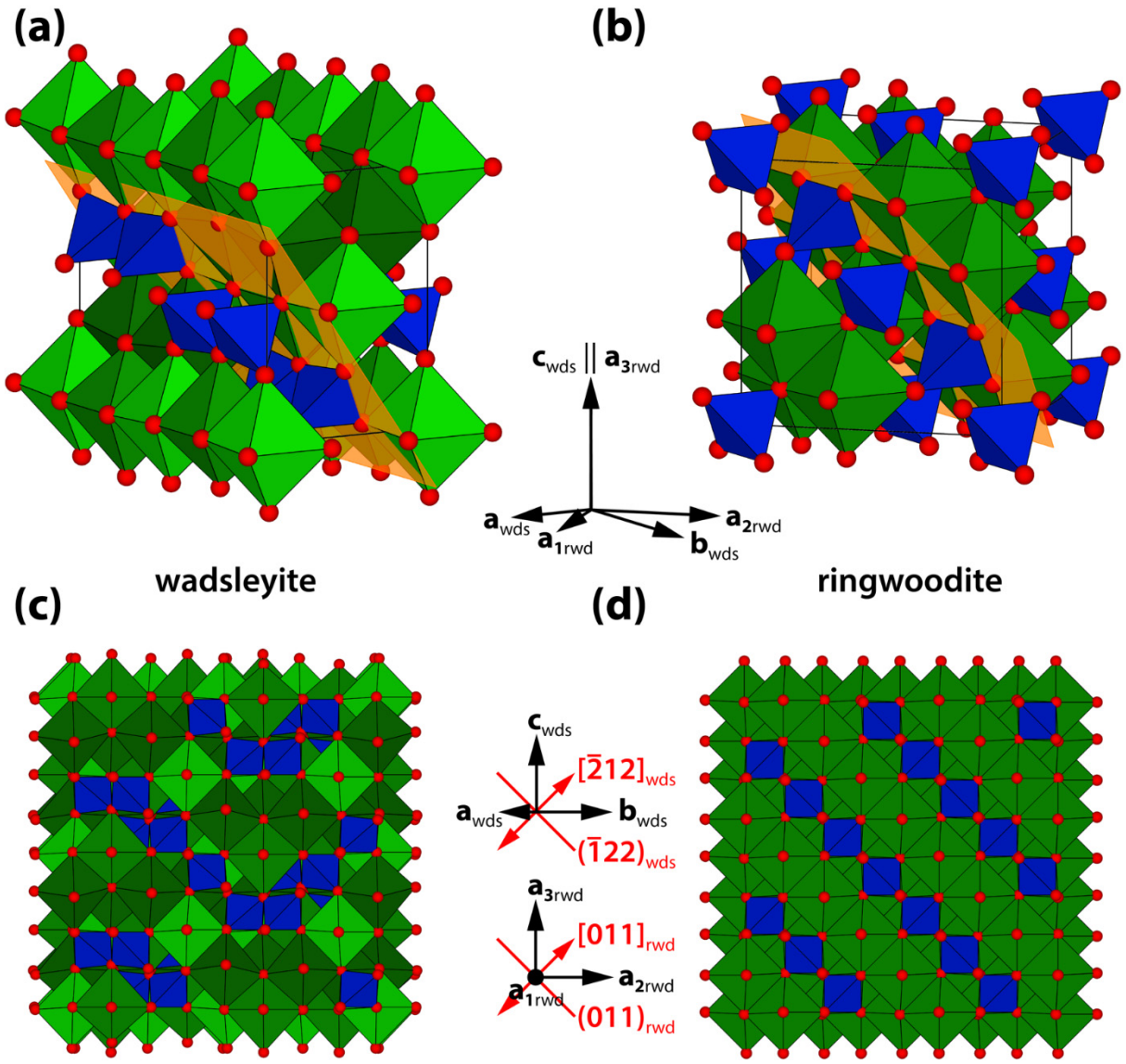

Fig. 8

Fig. 8. Depiction of the crystal structures of wadsleyite (a,c) and ringwoodite (b,d). Red spheres show oxygen anions; blue tetrahedra host silicon cations; green octahedra host magnesium and iron cations. The axis systems and crystal structures are drawn to preserve the orientational relationship between both crystal structures. In (a) and (b), orange planes indicate the orientation of close-packed layers of oxygen anions. In (c) and (d), the crystal structures of wadsleyite and

ringwoodite are projected along the $(\bar{1}22)_{wds}$ and $(011)_{rwd}$ planes, respectively, to highlight structural similarities. The orientation of twin axes and twin planes with respect to the axis systems of both crystal structures is indicated in red. Graphics were created with *VESTA* (Momma and Izumi, 2011).